Hindawi
Shock and Vibration
Volume 2018, Article ID 4535871, 21 pages
https://doi.org/10.1155/2018/4535871

Research Article

An Accurate Solution Method for the Static and Vibration Analysis of Functionally Graded Reissner-Mindlin Rectangular Plate with General Boundary Conditions

Haichao Li, Ning Liu, Fuzhen Pang, Yuan Du, and Shuo Li

College of Shipbuilding Engineering, Harbin Engineering University, Harbin 150001, China

Correspondence should be addressed to Ning Liu; liuning@hrbeu.edu.cn

Received 30 January 2018; Accepted 2 May 2018; Published 27 June 2018

Academic Editor: Tai Thai

This paper presents an accurate solution method for the static and vibration analysis of functionally graded Reissner-Mindlin plate with general boundary conditions on the basis of the improved Fourier series method. In the theoretical formulations, the governing equations and the general elastic boundary equations are obtained by using Hamilton's principle. The components of admissible displacement functions are expanded as an improved Fourier series form which contains a 2D Fourier cosine series and auxiliary function in the form of 1D series. The major role of the auxiliary function is to remove the potential discontinuities of the displacement function and its derivatives at the edges and ensure and accelerate the convergence of the series representation. The characteristic equations are easily obtained via substituting admissible displacement functions into governing equations and the general elastic boundary equations. Several examples are made to show the excellent accuracy and convergence of the current solutions. The results of this paper may serve as benchmark data for future research in related field.

1. Introduction

The concept of functionally graded materials (FGMs) was firstly presented in 1987 by a group of material scientists in Sendai region of Japan during the first five-year project to study relaxation of thermal stress of materials in high speed aerospace vehicle [1, 2]. Since then, FGMs have received the major attention as heat-shielding advanced structural materials in a variety of engineering applications and manufacturing industries, like aerospace, nuclear reactor automobile, aircraft, space vehicles, and biomedical and steel industries. The remarkable mechanical properties of the FGMs are achieved by gradually varying the volume fraction of the constituent materials whose properties vary from one interface to the other continuously.

As a most common infrastructure, the functionally graded rectangular plate has been widely used in practical engineering applications, i.e., aerospace, naval vessels, nuclear reactor, automobile, robot, and civil industries. On one hand, the research of static and vibration analysis of FG plate could provide the theoretical basis for practical engineering applications. On the other hand, the results of this paper could serve as the reference data in practical engineering applications in related field in future. The static and vibration analysis of the FG plate has been investigated by a large number of researches in the past decade. Among those available, Abrate [3] used the CPT to study the free vibration of FG thin rectangular plates with simply supported and clamped boundary conditions. Later, the free vibration, buckling and static deflections of FG square, and circular and skew plates with different combinations of boundary conditions were analyzed by Abrate [4] using the same method on the basis of the CPT, FSDT, and TSDT. Free and forced vibration analyses of both homogeneous and FG thick plates with classical boundary conditions were carried out by Qian et al. [5, 6] using the meshless local Petrov–Galerkin method based on the higher-order shear and normal deformable plate theory. Pradyumna and Bandyopadhyay [7] used the higher-order finite element method to investigate the free vibration of FG square plates with simply supported boundary condition. Ferreira et al. [8] employed the global collocation method and approximated the trial

solution with multiquadric radial basis functions to study the free vibration of FG square plates with different classical boundary conditions on the basis of the FSDT and third-order shear deformation plate theory (TSDT). Praveen and Reddy [9] used the finite element method to obtain the static and dynamic thermoelastic behavior of the FG plates with some selected classical boundary conditions. Based on the third-order shear deformation theory and Reddy von Karman-type geometric nonlinearity theory, Reddy [10] carried out the static linear analysis and nonlinear static and dynamic analysis by using the finite element method. Croce and Venini [11] presented a new method of finite elements for analyzing Reissner-Mindlin FG plates with classical boundary condition. Cheng and Batra [12, 13] applied the first-order shear deformation theory and a third-order shear deformation theory to study the static, buckling, and steady state vibrations of FG polygonal plate with simply supported boundary conditions. Zhao et al. [14] extended the element free *kp*-Ritz method to study the free vibration analysis for FG square and skew plates with different boundary conditions on the basis of the FSDT. The nonlinear free vibration behavior of FG square thin plates was analyzed by Woo et al. [15] by presenting an analytical solution on the basis of the von Karman theory. Based on the CPT, Yang and Shen [16] presented an analytical method for free vibration and transient response of initially stressed FG rectangular thin plates resting on Pasternak elastic foundation having classical boundary condition subjected to impulsive lateral loads. Later, Yang and Shen [17] used a semianalytical approach to investigate the dynamic behavior of FG plates with impulsive lateral loads and complicated environment. Zhong and Yu [18] employed a state-space approach to analyze free and forced vibrations of an FG piezoelectric rectangular thick plate with simple support at its edges. Roque et al. [19] employed the multiquadric radial basis function method and the HSDT to study free vibration of FG plates with different classical boundary conditions. The natural frequencies and buckling stresses of FG plates having simply supported edges were studied by Matsunaga [20] who utilized the method of power series expansion and two-dimensional (2D) higher-order theory. Hosseini-Hashemi et al. [21, 22] presented a new exact closed-form procedure for free vibration analysis of FG rectangular thick plates and Reissner-Mindlin FG rectangular plates where the plate has two opposite edges of simply supported boundary conditions. Vel and Batra [23] presented an exact 3-D elasticity solution to study the thermoelastic deformation, free and forced vibrations of FG simply supported plates. Based on the higher-order shear and normal deformation theory, Shiyekar et al. [24] presented the bidirectional flexure analysis of smart FG plate subjected to electromechanical loading by using Navier's technique. Carrera et al. [25] evaluated the effect of thickness stretching in plate/shell structures made by materials which are functionally graded (FGM) in the thickness direction according to Carrera's Unified Formulation. Based on Carrera's Unified Formulation, Neves et al. [26] presented explicit governing equations to study static and free vibration analysis of FGM plates by using meshless technique based on collocation with radial basis functions. Zhang et al. [27] used the local Kriging meshless method to study the mechanical and thermal buckling behaviors of ceramic–metal functionally grade plates subject the classical boundary conditions. Belabed et al. [28] presented an efficient and simple higher-order shear and normal deformation theory for the bending and free vibration analysis of FG simply supported plates. Thai and Vo [29–34] extended a simple shear deformation theory to study the bending, buckling, and vibration of functionally graded plates with simply supported cases. Valizadeh et al. [35] applied isogeometric finite element method to study the static and dynamic characteristics of functionally graded material (FGM) plates with classical boundary condition. Based on isogeometric approach (IGA) and higher-order deformation plate theory (HSDT), Tran et al. [36] used the C^1 continuous element to investigate the static, dynamic, and buckling analysis of FG rectangular and circular plates with different classical boundary conditions. Mantari et al. [37] showed an analytical solution to static analysis of functionally graded plates (FGPs) based on a new trigonometric higher-order theory in which the stretching effect was considered. Xiang and Kang [38] conducted bending analysis for functionally graded plates according to a nth-order shear deformation theory and the meshless global collocation method based on the thin plate spline radial basis function and Reddy's third-order theory. Based on various plate theory, Tornabene et al. [39] applied the Generalized Differential Quadrature (GDQ) to study the bending, vibration, and dynamic analysis of FG plates and panels with different classical boundary conditions. Xuan et al. [40] presented a simple and effective approach which incorporated the isogeometric finite element analysis (IGA) with a refined plate theory (RPT) for static, free vibration, and buckling analysis of functionally graded material (FGM) plates with simply supported and clamped boundary conditions. Akavci [41] presented a closed-form solution to study the free vibration analysis of functionally graded plate resting on Pasternak (two-parameter) model subject to classical boundary condition.

From the above review, we can know that most of existing literatures on the static and vibration analysis of functionally graded Reissner-Mindlin plate are restricted to the classical boundary condition. However, the elastic edge restraints may be more common in the practical engineering, and the classical boundary condition is considered as a special case. Thus, to establish a unified, efficient and accurate formulation for static and vibration analysis of functionally graded Reissner-Mindlin plate is necessary and significant.

To the best of author's knowledge, the subject of static and vibration analysis of functionally graded Reissner-Mindlin plate with general boundary conditions has not been performed in a specified work, yet. Therefore, the major focus of this paper is to present an accurate solution method for the static and vibration analysis of functionally graded Reissner-Mindlin plate with general boundary conditions. The effective material properties of functionally graded materials are assumed to vary continuously in the thickness direction according to the power-law distribution in terms of the volume fraction of the constituents and are estimated by the Voigt model and Mori–Tanaka scheme. All the plate displacements are expanded as a modified Fourier series

which is made up of a standard cosine Fourier series and some certain supplementary terms whatever the boundary conditions are. These supplementary terms contribute to removing the potential discontinuities at the edges and then ensure and accelerate the series convergence. The characteristic equations can be derived directly by solving the equation of motion and by combining the associated boundary equations and the modified Fourier series. The characteristic equations are easily obtained via substituting related modified Fourier series into governing equations and the general elastic boundary equations. A large number of numerical examples are made to show the convergence, reliability, and accuracy of the present method.

2. Theoretical and Numerical Formulations

2.1. Geometrical Configuration. Consider a flat and moderately thick FG plate with a with uniform thickness h, length a, and width b of plate in the z-, x-, and y-direction, as shown in Figure 1. In addition, the coordinate system (x, y, z) is also shown in Figure 1, which will be used in the analysis. The arbitrary boundary technique [43–47] is introduced to implement the general boundary condition in which one group of liner spring k_w^γ ($\gamma = x0, xa, y0$, and yb denote the location of the spring; i.e., $x0$ represents the location of the edge $x = 0$) and two groups of rotation springs K_x^γ and K_{xy}^γ are introduced to simulate the related boundary forces in each boundary of a plate, as shown in Figure 1. The general boundary condition is easily obtained by assigning the stiffness of the boundary springs with various values. Take the clamped boundary condition as an example; when the spring stiffness is set larger enough than the bending rigidity of plate, it can be obtained essentially. In addition, a common uniform pressure $q = q_0$ is acted on the rectangular area $[(x_1, x_2), (y_1, y_2)]$, and when the acting area is narrowed down to a point, a special case named the point load will be obtained, as illustrated in Figure 1.

2.2. Material Properties. It is supposed that the FGM of plate is made of two material constituents. In this study, the top surface ($z = h/2$) of the plate is ceramic-rich (Mc) whereas the bottom surface ($z = -h/2$) is metal-rich (Mm). Both the Voigt model and Mori–Tanaka scheme are adopted to evaluate the effective material properties [48]. In the Voigt model, it is assumed that the material properties including Young's modulus $E(z)$, density $\rho(z)$, and Poisson's ratio $\mu(z)$ are proportional to the volume fraction according to

$$\begin{aligned} E(z) &= (E_c - E_m) V_c(z) + E_m \\ \rho(z) &= (\rho_c - \rho_m) V_c(z) + \rho_m \\ \mu(z) &= (\mu_c - \mu_m) V_c(z) + \mu_m \end{aligned} \tag{1}$$

in which the subscripts m and c represent the metallic and ceramic constituents, respectively.

Based on the Mori–Tanaka scheme, the effective local bulk modulus K_c and the shear modulus G_c of the FGM plate can be expressed as

$$\begin{aligned} \frac{K - K_m}{K_c - K_m} &= \frac{V_c(z)}{1 + (1 - V_c(z))(K_c - K_m)/(K_m + 4G_m/3)} \\ \frac{G - G_m}{G_c - G_m} &= \frac{V_c(z)}{1 + (1 - V_c(z))(G_c - G_m)/\{(G_m + G_m(9K_m + 8G_m)/[6(K_m + 2G_m)])\}} \end{aligned} \tag{2}$$

where $K_i = E_i/[3(1-2\mu_i)]$ and $G_i = E_i/[2(1+2\mu_i)]$ $(i = m, c)$. The effective mass density which is defined by (1) is also utilized in the Mori–Tanaka scheme. The effective Young's modulus $E(z)$ and Poisson's ratio $\mu(z)$ are

$$\begin{aligned} E(z) &= \frac{9KG}{3K + G}, \\ \mu(z) &= \frac{3K - 2G}{6K + 2G} \end{aligned} \tag{3}$$

In the above FG scheme, the common volume fraction Vc may be given by

$$V_c = \begin{cases} \left[1 - e\left(\frac{1}{2} + \frac{z}{h}\right) + f\left(\frac{1}{2} + \frac{z}{h}\right)^g\right]^p \\ \left[1 - e\left(\frac{1}{2} - \frac{z}{h}\right) + f\left(\frac{1}{2} - \frac{z}{h}\right)^g\right]^p \end{cases} \tag{4}$$

where z is the thickness coordinate and p denotes the power-law exponent and only takes the positive values. The material parameters e, f, and g determine the material variation profile through the functionally graded plate thickness. It should be noted that, in order to make the results become more universal in the future, the authors just choose the Voigt model and material parameters of the volume fraction Vc are given as $e = 1$ and $f = 0$. The variations of volume fraction V_c for different values of the parameters e, f, g, and p are depicted in Figure 2.

2.3. Governing Equations and Boundary Conditions. Based on the Mindlin plate theory, the displacement components of the plate are assumed to be

$$\begin{aligned} u(x, y, z) &= z\varphi_x(x, y), v(x, y, z) \\ &= z\varphi_y(x, y), w(x, y, z) = w(x, y) \end{aligned} \tag{5}$$

where w is the displacements of the middle surface in z directions and ψ_x and ψ_y are the rotation functions. Following assumptions of the small deformation and the

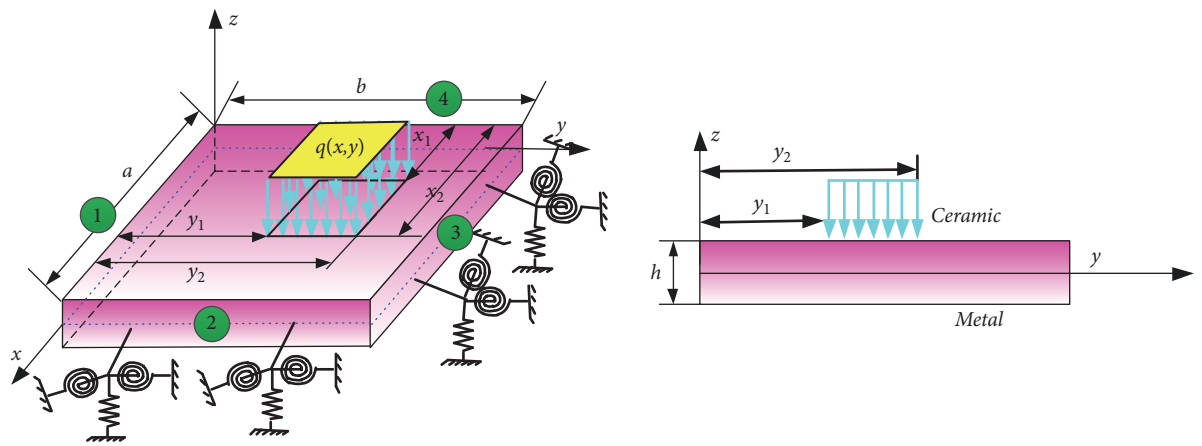

FIGURE 1: Schematic diagram of a FG Mindlin plate with elastically restrained edges.

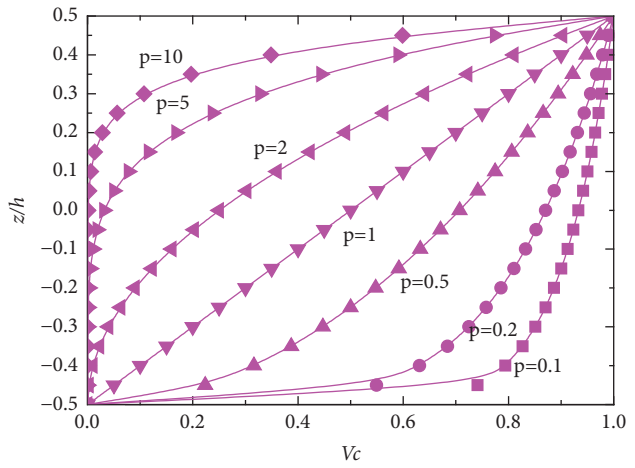

FIGURE 2: Variation of volume fraction Vc through the thickness for different values of power-law exponent.

linear strain–displacement relation, the strain components of FG plates can be written as

$$\varepsilon_x = z\frac{\partial \varphi_x}{\partial x} = z\kappa_x,$$
$$\varepsilon_y = z\frac{\partial \varphi_y}{\partial y} = z\kappa_y, \tag{6a}$$
$$\gamma_{xy} = z\left(\frac{\partial \varphi_y}{\partial x} + \frac{\partial \varphi_x}{\partial y}\right) = z\kappa_{xy}$$
$$\gamma_{xz} = \frac{\partial w}{\partial x} + \varphi_x, \tag{6b}$$
$$\gamma_{yz} = \frac{\partial w}{\partial y} + \varphi_y$$

According to Hook's law, the stress components of FG plates can be expressed as

$$\begin{Bmatrix} \sigma_x \\ \sigma_y \\ \tau_{xy} \\ \tau_{xz} \\ \tau_{yz} \end{Bmatrix} = \begin{bmatrix} Q_{11}(z) & Q_{12}(z) & 0 & 0 & 0 \\ Q_{12}(z) & Q_{11}(z) & 0 & 0 & 0 \\ 0 & 0 & Q_{66}(z) & 0 & 0 \\ 0 & 0 & 0 & Q_{66}(z) & 0 \\ 0 & 0 & 0 & 0 & Q_{66}(z) \end{bmatrix} \begin{Bmatrix} \varepsilon_x \\ \varepsilon_y \\ \gamma_{xy} \\ \gamma_{xz} \\ \gamma_{yz} \end{Bmatrix} \tag{7}$$

where the elastic constants $Q_{ij}(z)$ are the functions of thickness coordinate z:

$$Q_{11}(z) = \frac{E(z)}{1-\mu^2(z)},$$
$$Q_{12}(z) = \frac{\mu(z)E(z)}{1-\mu^2(z)}, \tag{8}$$
$$Q_{66}(z) = \frac{E(z)}{2[1+\mu(z)]}$$

By carrying the integration of the stresses over the cross-section, the force and moment resultants are written as follows:

$$M_x = D_{11}\frac{\partial \varphi_x}{\partial x} + D_{12}\frac{\partial \varphi_y}{\partial y},$$
$$M_y = D_{12}\frac{\partial \varphi_x}{\partial x} + D_{11}\frac{\partial \varphi_y}{\partial y},$$
$$M_{xy} = D_{66}\left(\frac{\partial \varphi_y}{\partial x} + \frac{\partial \varphi_x}{\partial y}\right)$$

$$Q_x = A_{66}\left(\frac{\partial w}{\partial x} + \varphi_x\right),$$
$$Q_y = A_{66}\left(\frac{\partial w}{\partial y} + \varphi_y\right) \tag{9}$$

where A_{ij} and D_{ij} are the extensional, bending stiffness, and they are, respectively, expressed as

$$\left(A_{66}, D_{11}, D_{22}, D_{12}\right) = \int_{-h/2}^{h/2}\left(\kappa Q_{66}(z), Q_{11}(z) \cdot z^2, Q_{11}(z) z^2, Q_{12}(z) z^2\right) dz \tag{10}$$

The strain energy and kinetic energy of the FG plate can be described as

$$U = \frac{1}{2}\int_0^a\int_0^b\left(\kappa_x M_x + \kappa_y M_y + \kappa_{xy} M_{xy} + \gamma_{xz} Q_x + \gamma_{yz} Q_y\right) dxdy = \frac{1}{2}\int_0^a\int_0^b\left(M_x\frac{\partial \varphi_x}{\partial x} + M_y\frac{\partial \varphi_y}{\partial y} + M_{xy}\left(\frac{\partial \varphi_x}{\partial y} + \frac{\partial \varphi_y}{\partial x}\right) + \left(\frac{\partial w}{\partial x} + \varphi_x\right)Q_x + \left(\frac{\partial w}{\partial y} + \varphi_y\right)Q_y\right) dxdy \tag{11}$$

$$T = \frac{1}{2}\int_0^a\int_0^b\left[I_0\left(\frac{\partial w}{\partial t}\right)^2 + I_2\left(\left(\frac{\partial \varphi_x}{\partial t}\right)^2 + \left(\frac{\partial \varphi_y}{\partial t}\right)^2\right)\right] dxdy, \tag{12}$$

$$\left[I_0 \;\; I_1\right] = \int_{-h/2}^{h/2}\rho\left(1 \;\; z^2\right) dz$$

In this paper, to develop a unified solution of the FG plate subjected to general elastic restrains, the static and vibration analysis is focused. So, the strain energy stored in the boundary springs during vibration can be defined as

$$\begin{aligned} V = {} & \frac{1}{2}\int_0^a\left(k_y^{y0} w^2 + K_{yx}^{y0}\varphi_x^2 + K_y^{y0}\varphi_y^2\right)\Big|_{y=0} dx \\ & + \frac{1}{2}\int_0^a\left(k_y^{yb} w^2 + K_{yx}^{yb}\varphi_x^2 + K_y^{yb}\varphi_y^2\right)\Big|_{y=b} dx \\ & + \frac{1}{2}\int_0^b\left(k_x^{x0} w^2 + K_x^{x0}\varphi_x^2 + K_{xy}^{x0}\varphi_y^2\right)\Big|_{x=0} dy \\ & + \frac{1}{2}\int_0^b\left(k_x^{xa} w^2 + K_x^{xa}\varphi_x^2 + K_{xy}^{xa}\varphi_y^2\right)\Big|_{x=a} dy \end{aligned} \tag{13}$$

Also, the external force on the plate during vibration can be defined as

$$W = \iint_A q(x, y) w(x, y) dA \tag{14}$$

To determine the static deflection, the load function should be expressed as a Fourier cosine series and the detailed information can be seen in [49].

The Lagrangian energy functional (L) of the plate is written as

$$L = T + W - U - V \tag{15}$$

Within arbitrary length of time, 0 to t_0, Hamilton's principle can be stated as follows:

$$\int_0^{t_0}(\delta T + \delta W - \delta U - \delta V) dt = 0 \tag{16}$$

By substituting (11)–(14) into (16), the variation equation can be rewritten as

$$\begin{aligned} & \int_0^{t_0}\int_0^a\int_0^b\left(-\frac{\partial M_x}{\partial x}\delta\varphi_x - \frac{\partial M_{r\theta}}{\partial y}\delta\varphi_x + Q_x\delta\varphi_x - \frac{\partial M_y}{\partial y}\delta\varphi_y - \frac{\partial M_{xy}}{\partial x}\delta\varphi_y + Q_y\delta\varphi_y - \frac{\partial Q_x}{\partial x}\delta w + -\frac{\partial Q_y}{\partial y}\delta w\right) dxdydt \\ & \int_0^{t_0}\int_0^a\left(M_{xy}\delta\varphi_x\Big|_{y=0}^{y=b} + Q_y\delta w\Big|_{y=0}^{y=b} + M_y\delta\varphi_y\Big|_{y=0}^{y=b}\right) dxdt + \int_0^{t_0}\int_0^b\left(M_x\delta\varphi_x\Big|_{x=0}^{x=a} + Q_x\delta w\Big|_{x=0}^{x=a} + M_{xy}\delta\varphi_y\Big|_{x=0}^{x=a}\right) dydt \\ & \int_0^{t_0}\int_0^a\left(k_y^{y0} w\delta w + K_{yx}^{y0}\varphi_x\delta\varphi_x + K_y^{y0}\varphi_y\delta\varphi_y\right)\Big|_{y=0} dxdt + \int_0^{t_0}\int_0^a\left(k_y^{yb} w\delta w + K_{yx}^{yb}\varphi_x\delta\varphi_x + K_y^{yb}\varphi_y\delta\varphi_y\right)\Big|_{y=b} dxdt \\ & + \int_0^{t_0}\int_0^b\left(k_x^{x0} w\delta w + K_x^{x0}\varphi_x\delta\varphi_x + K_{xy}^{x0}\varphi_y\delta\varphi_y\right)\Big|_{x=0} dydt + \int_0^{t_0}\int_0^b\left(k_x^{xa} w\delta w + K_x^{xa}\varphi_x\delta\varphi_x + K_{xy}^{xa}\varphi_y\delta\varphi_y\right)\Big|_{x=a} dydt \\ & + \int_0^{t_0}\int_0^a\int_0^b\left[I_0\left(\frac{\partial w}{\partial t}\right)^2\delta w + I_2\left(\left(\frac{\partial \varphi_x}{\partial t}\right)^2\delta\varphi_x + \left(\frac{\partial \varphi_y}{\partial t}\right)^2\delta\varphi_y\right)\right] dxdydt - \int_0^{t_0}\int_0^a\int_0^b q(x, y)\delta w dxdydt = 0 \end{aligned} \tag{17}$$

Integrating by parts to relieve the virtual displacements $\delta\varphi_x$, $\delta\varphi_y$, and δw, we have

$$\int_0^{t_0}\int_0^a\int_0^b \begin{pmatrix} \left\{-\frac{\partial M_x}{\partial x}-\frac{\partial M_{xy}}{\partial y}+Q_x+I_2\left(\frac{\partial \varphi_x}{\partial t}\right)^2\right\}\delta\varphi_x \\ \left\{-\frac{\partial M_y}{\partial y}-\frac{\partial M_{xy}}{\partial x}+Q_y+I_2\left(\frac{\partial \varphi_y}{\partial t}\right)^2\right\}\delta\varphi_y \\ \left\{-\frac{\partial Q_x}{\partial x}-\frac{\partial Q_y}{\partial y}-q+I_0\left(\frac{\partial w}{\partial t}\right)^2\right\}\delta w \end{pmatrix} dxdydt$$
$$+\int_0^{t_0}\int_0^a \left(\left(k_y^{y0}w-Q_y\right)\delta w+\left(K_{yx}^{y0}\varphi_x-M_{xy}\right)\delta\varphi_x+\left(K_y^{y0}\varphi_y-M_y\right)\delta\varphi_y\right)\Big|_{y=0}dxdt$$
$$+\int_0^{t_0}\int_0^a \left(\left(k_y^{yb}w+Q_y\right)\delta w+\left(K_{yx}^{yb}\varphi_x+M_{xy}\right)\delta\varphi_x+\left(K_y^{yb}\varphi_y+M_y\right)\delta\varphi_y\right)\Big|_{y=b}dxdt$$
$$+\int_0^{t_0}\int_0^b \left(\left(k_x^{x0}w-Q_x\right)\delta w+\left(K_x^{x0}\varphi_x-M_x\right)\delta\varphi_x+\left(K_{xy}^{x0}\varphi_y-M_{xy}\right)\delta\varphi_y\right)\Big|_{x=0}dydt$$
$$+\int_0^{t_0}\int_0^b \left(\left(k_x^{xa}w+Q_x\right)\delta w+\left(K_x^{xa}\varphi_x+M_x\right)\delta\varphi_x+\left(K_{xy}^{xa}\varphi_y+M_{xy}\right)\delta\varphi_y\right)\Big|_{x=a}dydt=0 \tag{18}$$

Since the virtual displacements $\delta\varphi_x$, $\delta\varphi_y$, and δw are arbitrary, (18) can be satisfied only if the coefficients of the virtual displacements are zero. Thus, the governing equation of motion and general boundary conditions for the static and vibration analysis of a FG plate can be derived as

$$\frac{\partial M_x}{\partial x}+\frac{\partial M_{xy}}{\partial y}-Q_x-I_2\left(\frac{\partial \varphi_x}{\partial t}\right)^2=0$$
$$\frac{\partial M_y}{\partial y}+\frac{\partial M_{xy}}{\partial x}-Q_y-I_2\left(\frac{\partial \varphi_y}{\partial t}\right)^2=0 \tag{19}$$
$$\frac{\partial Q_x}{\partial x}+\frac{\partial Q_y}{\partial y}+q(x,y)-I_0\left(\frac{\partial w}{\partial t}\right)^2=0$$

$$x=0:$$
$$K_x^{x0}\varphi_x=M_x,$$
$$K_{xy}^{x0}\varphi_y=M_{xy},$$
$$k_x^{x0}w=Q_x$$
$$x=a:$$
$$K_x^{xa}\varphi_x=-M_x,$$
$$K_{xy}^{xa}\varphi_y=-M_{xy},$$
$$k_x^{xa}w=-Q_x$$
$$y=0:$$
$$K_y^{y0}\varphi_y=M_y,$$
$$K_{yx}^{y0}\varphi_x=M_{xy},$$
$$k_y^{y0}w=Q_y$$
$$y=b:$$
$$K_y^{yb}\varphi_y=-M_y,$$
$$K_{yx}^{yb}\varphi_x=-M_{xy},$$
$$k_y^{yb}w=-Q_y \tag{20}$$

Further, substituting (6a), (6b), and (9) into (19) and (20), the governing equation of motion can be expressed in matrix form:

$$\left(\begin{bmatrix} L_{11} & L_{12} & L_{13} \\ L_{21} & L_{22} & L_{23} \\ L_{31} & L_{32} & L_{33} \end{bmatrix}-\omega^2\begin{bmatrix} M_{11} & 0 & 0 \\ 0 & M_{22} & 0 \\ 0 & 0 & M_{33} \end{bmatrix}\right)\begin{bmatrix} \varphi_x \\ \varphi_y \\ w \end{bmatrix}=\begin{bmatrix} 0 \\ 0 \\ q \end{bmatrix} \tag{21}$$

where

$$
\begin{aligned}
L_{11} &= D_{11}\frac{\partial^2}{\partial x^2} - A_{66} + D_{66}\frac{\partial^2}{\partial y^2},\\
L_{12} &= D_{12}\frac{\partial^2}{\partial x\partial y} + D_{66}\frac{\partial^2}{\partial x\partial y},\\
L_{13} &= -A_{66}\frac{\partial}{\partial x}\\
L_{21} &= D_{12}\frac{\partial^2}{\partial x\partial y} + D_{66}\frac{\partial^2}{\partial x\partial y},\\
L_{22} &= D_{66}\frac{\partial^2}{\partial x^2} - A_{66} + D_{11}\frac{\partial^2}{\partial y^2},\\
L_{23} &= -A_{66}\frac{\partial}{\partial y}\\
L_{31} &= A_{66}\frac{\partial}{\partial x},\\
L_{32} &= A_{66}\frac{\partial}{\partial y},\\
L_{33} &= A_{66}\frac{\partial^2}{\partial x^2} + A_{66}\frac{\partial^2}{\partial y^2},\\
M_{11} &= M_{22} = I_2,\\
M_{33} &= I_0
\end{aligned}
\tag{22}
$$

Similarly, the general boundary conditions can be written as

$$
\begin{bmatrix} L_{11}^j & L_{12}^j & L_{13}^j \\ L_{21}^j & L_{22}^j & L_{23}^j \\ L_{31}^j & L_{32}^j & L_{33}^j \end{bmatrix} \begin{bmatrix} \varphi_x \\ \varphi_y \\ w \end{bmatrix} = \begin{bmatrix} 0 \\ 0 \\ 0 \end{bmatrix}, \quad \left(j = x0, xa, y0, y\mathrm{b}\right) \tag{23}
$$

where

$$
\begin{aligned}
L_{11}^{x0} &= D_{11}\frac{\partial}{\partial x} - K_x^{x0},\\
L_{12}^{x0} &= D_{12}\frac{\partial}{\partial y},\\
L_{13}^{x0} &= 0,\\
L_{21}^{x0} &= D_{66}\frac{\partial}{\partial y},\\
L_{22}^{x0} &= D_{66}\frac{\partial}{\partial x} - K_{xy}^{x0},\\
L_{23}^{x0} &= 0\\
L_{31}^{x0} &= A_{66},\\
L_{32}^{x0} &= 0,\\
L_{33}^{x0} &= A_{66}\frac{\partial}{\partial x} - k_x^{x0},\\
L_{11}^{y0} &= D_{66}\frac{\partial}{\partial y} - K_{yx}^{y0},\\
L_{12}^{y0} &= D_{66}\frac{\partial}{\partial x},\\
L_{13}^{y0} &= 0\\
L_{21}^{y0} &= D_{12}\frac{\partial}{\partial x},\\
L_{22}^{y0} &= D_{11}\frac{\partial}{\partial y} - K_y^{y0},\\
L_{23}^{y0} &= 0,\\
L_{31}^{y0} &= 0,\\
L_{32}^{y0} &= A_{66},\\
L_{33}^{y0} &= A_{66}\frac{\partial}{\partial y} - k_y^{y0}\\
L_{ij}^{x0} &= L_{ij}^{x1}, \quad (i \neq j),\\
L_{ij}^{y0} &= L_{ij}^{y1}, \quad (i \neq j),\\
L_{11}^{x1} &= D_{11}\frac{\partial}{\partial x} + K_x^{xa},\\
L_{22}^{x1} &= D_{66}\frac{\partial}{\partial x} + K_{xy}^{xa}\\
L_{33}^{x1} &= A_{66}\frac{\partial}{\partial x} + k_x^{xa},\\
L_{11}^{y1} &= D_{66}\frac{\partial}{\partial y} + K_{yx}^{yb},\\
L_{22}^{y1} &= D_{11}\frac{\partial}{\partial y} + K_y^{yb},\\
L_{33}^{y1} &= A_{66}\frac{\partial}{\partial y} + k_y^{yb}
\end{aligned}
\tag{24}
$$

2.4. Admissible Displacement Functions. In the structure vibration problem, the scope of boundary condition and the accuracy of the solution strongly depend on the choice of the admissible function of structures. Generally, for the commonly used polynomial expression, their convergence is uncertain. In other words, the lower-order polynomials cannot form a complete set, and, on the contrary, it may lead to be numerically unstable owing to the computer round-off errors when the higher-order polynomials are applied.

To avoid the above weakness, the admissible functions can be expanded as the form of Fourier series due to the excellent numerical stability of the Fourier series. However, the conventional Fourier series just adapt to a few of simple boundary conditions due to the convergence problem along the boundary conditions. Recently, a modified Fourier series technique proposed by Li [50] has been widely applied in the vibration problems of plates and shells subject to different boundary conditions by the Ritz method, e.g., [42, 51–60]. In this technique, each displacement of the structure under study is written in the form of a conventional cosine Fourier series and several supplementary terms. The detailed principle and merit of the improved Fourier series can be seen in the related book [61] (entitled "*Structural Vibration A Uniform Accurate Solution for Laminated Beams, Plates and Shells with General Boundary Conditions*"). On the basis of the modified Fourier series technique, Jin et al. [48, 62] present an exact series solution to study the free vibration of functionally graded sandwich beams, composite laminated deep curved beams, and so on. Compared with most of the existing methods, the exact series solution not only owns the excellent convergence and accuracy but also can be applied to general boundary conditions. Therefore, in this formulation, the modified Fourier series technique is adopted and extended to conduct the static and vibration analysis of functionally graded Reissner-Mindlin plate with general boundary conditions.

Combining (6a), (6b), (9), and (19), it can be known that each displacement/rotation component of a FG plate is required to have up to the second derivative. Therefore, no matter what the boundary conditions are, each displacement/rotation component of the plate is assumed to be a two-dimensional modified Fourier series as

$$\begin{aligned}
\varphi_x(x,y) &= \sum_{m=0}^{M}\sum_{n=0}^{N} A_{mn}\cos\lambda_{am}x\cos\lambda_{bn}y \\
&\quad + \sum_{l=1}^{2}\sum_{m=0}^{M} b_m^l \zeta_b^l(y)\cos\lambda_{am}x \\
&\quad + \sum_{l=1}^{2}\sum_{n=0}^{N} a_n^l \zeta_a^l(x)\cos\lambda_{bn}y \\
\varphi_y(x,y) &= \sum_{m=0}^{M}\sum_{n=0}^{N} B_{mn}\cos\lambda_{am}x\cos\lambda_{bn}y \\
&\quad + \sum_{l=1}^{2}\sum_{m=0}^{M} d_m^l \zeta_b^l(y)\cos\lambda_{am}x \\
&\quad + \sum_{l=1}^{2}\sum_{n=0}^{N} c_n^l \zeta_a^l(x)\cos\lambda_{bn}y \\
w(x,y) &= \sum_{m=0}^{M}\sum_{n=0}^{N} C_{mn}\cos\lambda_{am}x\cos\lambda_{bn}y \\
&\quad + \sum_{l=1}^{2}\sum_{m=0}^{M} f_m^l \zeta_b^l(y)\cos\lambda_{am}x \\
&\quad + \sum_{l=1}^{2}\sum_{n=0}^{N} e_n^l \zeta_a^l(x)\cos\lambda_{bn}y
\end{aligned} \tag{25}$$

where $\lambda_{am} = m\pi/a$, $\lambda_{bb} = n\pi/b$, and A_{mn}, B_{mn},and C_{mn} are the Fourier coefficients of two-dimensional Fourier series expansions for the displacements functions, respectively. M and N are the truncation numbers. ζ_a^l and ζ_b^l, $l = 1, 2$, represent the auxiliary functions defined over $\boldsymbol{D}$:$([0,a] \times [0,b])$ whose major role is to eliminate all the discontinuities potentially associated with the first-order derivatives at the boundary and then ensure and accelerate the convergence of the series expansion of the plate displacement. Here, it should be noted that the auxiliary functions just satisfy $\zeta_a^1(0) = \zeta_a^1(a) = \zeta_a^{1'}(a) = 0$, $\zeta_a^{1'}(0) = 1$ and $\zeta_a^2(0) = \zeta_a^2(a) = \zeta_a^{2'}(0) = 0$, and $\zeta_a^{2'}(a) = 1$; however, the concrete form is not the focus of attention. a_m^l, b_n^l, c_m^l, d_n^l, e_m^l, and f_n^l are the corresponding supplemented coefficients of the auxiliary functions, where $l = 1, 2$. Those auxiliary functions are defined as follows:

$$\begin{aligned}
\zeta_a^1(x) &= \frac{a}{2\pi}\sin\left(\frac{\pi x}{2a}\right) + \frac{a}{2\pi}\sin\left(\frac{3\pi x}{2a}\right), \\
\zeta_a^2(x) &= -\frac{a}{2\pi}\cos\left(\frac{\pi x}{2a}\right) + \frac{a}{2\pi}\cos\left(\frac{3\pi x}{2a}\right) \\
\zeta_b^1(y) &= \frac{b}{2\pi}\sin\left(\frac{\pi y}{2b}\right) + \frac{b}{2\pi}\sin\left(\frac{3\pi y}{2b}\right), \\
\zeta_b^2(y) &= -\frac{b}{2\pi}\cos\left(\frac{\pi y}{2b}\right) + \frac{b}{2\pi}\cos\left(\frac{3\pi y}{2b}\right)
\end{aligned} \tag{26}$$

Further, the modified Fourier series expressions presented in (25) can be rewritten in the matrix form as

$$\begin{aligned}
\varphi_x(x,y) &= \mathbf{H}_{xy}\mathbf{A} + \mathbf{H}_x\mathbf{a} + \mathbf{H}_y\mathbf{b} \\
\varphi_y(x,y) &= \mathbf{H}_{xy}\mathbf{B} + \mathbf{H}_x\mathbf{c} + \mathbf{H}_y\mathbf{d} \\
w(x,y) &= \mathbf{H}_{xy}\mathbf{C} + \mathbf{H}_x\mathbf{e} + \mathbf{H}_y\mathbf{f}
\end{aligned} \tag{27}$$

where

$$\begin{aligned}
\mathbf{H}_{xy} &= [\cos\lambda_{a0}x\cos\lambda_{b0}y, \ldots, \cos\lambda_{am}x \\
&\quad \cdot \cos\lambda_{bn}y, \ldots, \cos\lambda_{aM}x\cos\lambda_{bN}y] \\
\mathbf{H}_x &= [\zeta_a^1(x)\cos\lambda_{b0}y, \ldots, \zeta_a^l(x)\cos\lambda_{bn}y, \ldots, \zeta_a^2(x) \\
&\quad \cdot \cos\lambda_{bN}y] \\
\mathbf{H}_y &= [\zeta_b^1(y)\cos\lambda_{a0}x, \ldots, \zeta_b^l(y)\cos\lambda_{am}x, \ldots, \zeta_b^2(y) \\
&\quad \cdot \cos\lambda_{aM}x] \\
\mathbf{A} &= [A_{00}, \cdots, A_{mn}, \cdots, A_{MN}]^T, \\
\mathbf{a} &= [a_0^1, \cdots, a_n^l, \cdots, a_N^2]^T, \\
\mathbf{b} &= [b_0^1, \cdots, b_m^l, \cdots, b_M^2]^T \\
\mathbf{B} &= [B_{00}, \cdots, B_{mn}, \cdots, B_{MN}]^T, \\
\mathbf{c} &= [c_0^1, \cdots, c_n^l, \cdots, c_N^2]^T,
\end{aligned}$$

$$\mathbf{d} = \left[d_0^1, \cdots, d_m^l, \cdots, d_M^2\right]^T$$
$$\mathbf{C} = \left[C_{00}, \cdots, C_{mn}, \cdots, C_{MN}\right]^T,$$
$$\mathbf{e} = \left[e_0^1, \cdots, e_n^l, \cdots, e_N^2\right]^T,$$
$$\mathbf{f} = \left[f_0^1, \cdots, f_m^l, \cdots, f_M^2\right]^T \tag{28}$$

2.5. Governing Eigenvalue Equations. Substituting (27) into (21) results in

$$\mathbf{L}_{xy}\boldsymbol{\Theta}_{xy} + \mathbf{L}_x\boldsymbol{\Theta}_x + \mathbf{L}_y\boldsymbol{\Theta}_y - \omega^2\left(\mathbf{M}_{xy}\boldsymbol{\Theta}_{xy} + \mathbf{M}_x\boldsymbol{\Theta}_x + \mathbf{M}_y\boldsymbol{\Theta}_y\right) = \mathbf{F} \tag{29}$$

where

$$\mathbf{L}_i = \begin{bmatrix} L_{11}\mathbf{H}_i & L_{12}\mathbf{H}_i & L_{13}\mathbf{H}_i \\ L_{21}\mathbf{H}_i & L_{22}\mathbf{H}_i & L_{23}\mathbf{H}_i \\ L_{31}\mathbf{H}_i & L_{32}\mathbf{H}_i & L_{33}\mathbf{H}_i \end{bmatrix}, \quad (i = xy, x, y)$$
$$\mathbf{M}_i = \begin{bmatrix} M_{11}\mathbf{H}_i & 0 & 0 \\ 0 & M_{22}\mathbf{H}_i & 0 \\ 0 & 0 & M_{33}\mathbf{H}_i \end{bmatrix}, \quad (i = xy, x, y) \tag{30}$$
$$\boldsymbol{\Theta}_{xy} = \left[\mathbf{A}\ \ \mathbf{B}\ \ \mathbf{C}\right]^T,$$
$$\boldsymbol{\Theta}_x = \left[\mathbf{a}\ \ \mathbf{c}\ \ \mathbf{e}\right]^T,$$
$$\boldsymbol{\Theta}_y = \left[\mathbf{b}\ \ \mathbf{d}\ \ \mathbf{f}\right]^T,$$
$$\mathbf{F} = \left[\mathbf{0}\ \ \mathbf{0}\ \ \mathbf{q}\right]^T$$

In the same way, substituting (27) into (23), the general boundary conditions of the plate can be rewritten as

$$\mathbf{L}_{xy}^j\boldsymbol{\Theta}_{xy} + \mathbf{L}_x^j\boldsymbol{\Theta}_x + \mathbf{L}_y^j\boldsymbol{\Theta}_y = 0, \quad (j = x0, y0, xa, yb) \tag{31}$$

where

$$\mathbf{L}_i^j = \begin{bmatrix} L_{11}^j\mathbf{H}_i & L_{12}^j\mathbf{H}_i & L_{13}^j\mathbf{H}_i \\ L_{21}^j\mathbf{H}_i & L_{22}^j\mathbf{H}_i & L_{23}^j\mathbf{H}_i \\ L_{31}^j\mathbf{H}_i & L_{32}^j\mathbf{H}_i & L_{33}^j\mathbf{H}_i \end{bmatrix}, \quad (i = xy, x, y,\ \ j = x0, y0, xa, yb) \tag{32}$$

To derive the constraint equations of the unknown Fourier coefficients, all the sine terms, the auxiliary polynomial functions, and their derivatives in (29) and (31) will be expanded into Fourier cosine series, letting

$$\mathbf{C}_{xy} = \left[\cos\lambda_{a0}x\cos\lambda_{b0}y, \cdots, \cos\lambda_{am}x \cdot \cos\lambda_{bn}y, \cdots, \cos\lambda_{aM}x\cos\lambda_{bN}y\right]$$
$$\mathbf{C}_x = \left[\cos\lambda_{a0}x, \cdots, \cos\lambda_{am}x, \cdots, \cos\lambda_{aM}x\right]$$
$$\mathbf{C}_y = \left[\cos\lambda_{b0}y, \cdots, \cos\lambda_{bn}y, \cdots, \cos\lambda_{bN}y\right] \tag{33}$$

Multiplying (29) with $\boldsymbol{C}_{xy}$ in the left side and integrating it from 0 to a and 0 to b separately with respect to x and y obtains

$$\overline{\mathbf{L}}_{xy}\boldsymbol{\Theta}_{xy} + \begin{bmatrix}\overline{\mathbf{L}}_x & \overline{\mathbf{L}}_y\end{bmatrix}\begin{bmatrix}\boldsymbol{\Theta}_x \\ \boldsymbol{\Theta}_y\end{bmatrix} - \omega^2\left(\overline{\mathbf{M}}_{xy}\boldsymbol{\Theta}_{xy} + \begin{bmatrix}\overline{\mathbf{M}}_x & \overline{\mathbf{M}}_y\end{bmatrix}\begin{bmatrix}\boldsymbol{\Theta}_x \\ \boldsymbol{\Theta}_y\end{bmatrix}\right) = \overline{\mathbf{F}} \tag{34}$$

where

$$\overline{\mathbf{L}}_{xy} = \int_0^a\int_0^b \mathbf{C}_{xy}\mathbf{L}_{xy}dxdy,$$
$$\overline{\mathbf{M}}_{xy} = \int_0^a\int_0^b \mathbf{C}_{xy}\mathbf{M}_{xy}dxdy$$
$$\overline{\mathbf{L}}_x = \int_0^a\int_0^b \mathbf{C}_{xy}\mathbf{L}_xdxdy,$$
$$\overline{\mathbf{M}}_x = \int_0^a\int_0^b \mathbf{C}_{xy}\mathbf{M}_xdxdy$$
$$\overline{\mathbf{L}}_y = \int_0^a\int_0^b \mathbf{C}_{xy}\mathbf{L}_ydxdy,$$
$$\overline{\mathbf{M}}_y = \int_0^a\int_0^b \mathbf{C}_{xy}\mathbf{M}_ydxdy \tag{35}$$

Similarly, multiplying (31) with $\boldsymbol{C}_y$ in the left side and then integrating it from 0 to b with respect to y along the edges $x = x0$ and xa and multiplying (31) with $\boldsymbol{C}_x$ in the left side and then integrating it from 0 to a with respect to x at the edges $y = y0$ and yb, we have

$$\overline{\mathbf{L}}_{xy}^j\boldsymbol{\Theta}_{xy} + \overline{\mathbf{L}}_x^j\boldsymbol{\Theta}_x + \overline{\mathbf{L}}_y^j\boldsymbol{\Theta}_y = 0, \quad (j = x0, y0, x1, y1) \tag{36}$$

where

$$\overline{\mathbf{L}}_{xy}^{x0} = \int_0^b \mathbf{C}_y\mathbf{L}_{xy}^{x0}dy,$$
$$\overline{\mathbf{L}}_{xy}^{xa} = \int_0^b \mathbf{C}_y\mathbf{L}_{xy}^{xa}dy$$
$$\overline{\mathbf{L}}_x^{x0} = \int_0^b \mathbf{C}_y\mathbf{L}_x^{x0}dy,$$
$$\overline{\mathbf{L}}_x^{xa} = \int_0^b \mathbf{C}_y\mathbf{L}_x^{xa}dy$$
$$\overline{\mathbf{L}}_y^{x0} = \int_0^b \mathbf{C}_y\mathbf{L}_y^{x0}dy,$$
$$\overline{\mathbf{L}}_y^{xa} = \int_0^b \mathbf{C}_y\mathbf{L}_y^{xa}dy,$$
$$\overline{\mathbf{L}}_{xy}^{y0} = \int_0^a \mathbf{C}_x\mathbf{L}_{xy}^{y0}dx,$$
$$\overline{\mathbf{L}}_{xy}^{yb} = \int_0^a \mathbf{C}_x\mathbf{L}_{xy}^{yb}dx$$

Table 1: Material properties used in the FG plate. Table 1 is reproduced from Wang [42] et al. (2017) (under the Creative Commons Attribution License/public domain).

Properties	Metal		Ceramic	
	Steel	Aluminum (Al)	Alumina (Al_2O_3)	Zirconia (ZrO_2)
E (Gpa)	207	70	380	200
μ	0.3	0.3	0.3	0.3
ρ (kg/m^3)	7800	2702	3800	5700

$$\begin{aligned}
\overline{\mathbf{L}}_x^{y0} &= \int_0^a \mathbf{C}_x \mathbf{L}_x^{y0} dx, \\
\overline{\mathbf{L}}_x^{yb} &= \int_0^a \mathbf{C}_x \mathbf{L}_x^{yb} dx \\
\overline{\mathbf{L}}_y^{y0} &= \int_0^a \mathbf{C}_x \mathbf{L}_y^{y0} dx, \\
\overline{\mathbf{L}}_y^{yb} &= \int_0^a \mathbf{C}_x \mathbf{L}_y^{yb} dx
\end{aligned} \tag{37}$$

Thus, (36) can be rewritten as

$$\begin{bmatrix} \boldsymbol{\Theta}_x \\ \boldsymbol{\Theta}_y \end{bmatrix} = \begin{bmatrix} \overline{\mathbf{L}}_x^{x0} & \overline{\mathbf{L}}_y^{x0} \\ \overline{\mathbf{L}}_x^{xa} & \overline{\mathbf{L}}_y^{xa} \\ \overline{\mathbf{L}}_x^{y0} & \overline{\mathbf{L}}_y^{y0} \\ \overline{\mathbf{L}}_x^{ya} & \overline{\mathbf{L}}_y^{yb} \end{bmatrix}^{-1} \begin{bmatrix} \overline{\mathbf{L}}_{xy}^{x0} \\ \overline{\mathbf{L}}_{xy}^{xa} \\ \overline{\mathbf{L}}_{xy}^{y0} \\ \overline{\mathbf{L}}_{xy}^{yb} \end{bmatrix} \boldsymbol{\Theta}_{xy} \tag{38}$$

Finally, combining (34) and (37) results in

$$\left(\mathbf{K} - \omega^2 \mathbf{M}\right) \boldsymbol{\Theta}_{xy} = \overline{\mathbf{F}} \tag{39}$$

where

$$\begin{aligned}
\mathbf{K} &= \overline{\mathbf{L}}_{xy} - \begin{bmatrix} \overline{\mathbf{L}}_x & \overline{\mathbf{L}}_y \end{bmatrix} \begin{bmatrix} \overline{\mathbf{L}}_x^{x0} & \overline{\mathbf{L}}_y^{x0} \\ \overline{\mathbf{L}}_x^{xa} & \overline{\mathbf{L}}_y^{xa} \\ \overline{\mathbf{L}}_x^{y0} & \overline{\mathbf{L}}_y^{y0} \\ \overline{\mathbf{L}}_x^{ya} & \overline{\mathbf{L}}_y^{yb} \end{bmatrix}^{-1} \begin{bmatrix} \overline{\mathbf{L}}_{xy}^{x0} \\ \overline{\mathbf{L}}_{xy}^{xa} \\ \overline{\mathbf{L}}_{xy}^{y0} \\ \overline{\mathbf{L}}_{xy}^{yb} \end{bmatrix}, \\
\mathbf{M} &= \overline{\mathbf{M}}_{xy} - \begin{bmatrix} \overline{\mathbf{M}}_x & \overline{\mathbf{M}}_y \end{bmatrix} \begin{bmatrix} \overline{\mathbf{L}}_x^{x0} & \overline{\mathbf{L}}_y^{x0} \\ \overline{\mathbf{L}}_x^{xa} & \overline{\mathbf{L}}_y^{xa} \\ \overline{\mathbf{L}}_x^{y0} & \overline{\mathbf{L}}_y^{y0} \\ \overline{\mathbf{L}}_x^{ya} & \overline{\mathbf{L}}_y^{yb} \end{bmatrix}^{-1} \begin{bmatrix} \overline{\mathbf{L}}_{xy}^{x0} \\ \overline{\mathbf{L}}_{xy}^{xa} \\ \overline{\mathbf{L}}_{xy}^{y0} \\ \overline{\mathbf{L}}_{xy}^{yb} \end{bmatrix}
\end{aligned} \tag{40}$$

In (40), $\mathbf{K}$ is the stiffness matrix for the plate and the $\mathbf{M}$ is the mass matrix. $\overline{\mathbf{F}}$ is the load vector. In the static analysis, the Fourier coefficients, $\boldsymbol{\Theta}_{xy}$, will be firstly solved from (39) by setting $\omega = 0$ and then the remaining Fourier coefficients will be calculated by using (38). The actual displacement function can then be easily determined from (37). While the load vector is equal to zero ($\overline{\mathbf{F}} = \mathbf{0}$), the vibration behavior which consists of the natural frequencies (or eigenvalues) and associated mode shapes (or eigenvectors) of FG plates can be readily obtained.

3. Numerical Results and Discussion

In order to demonstrate the present method, the static and free vibration analysis of FG plates with different boundary conditions will be considered in the following examples. Four types of material properties will be used in the following examples as seen in Table 1. For the purpose of describing the boundary condition sequence of the FG plate, a simple letter string is employed to simplify this study, as shown in Figure 1. The corresponding stiffness for the restraining springs is specified in Table 2. In addition, the new function of the shear correction factor will be introduced in the FG plate which can adapt to the actual model, and the detailed expression is defined as

$$\begin{aligned}
\kappa(p, \vartheta) = \frac{5}{6} &+ C_1 \left(e^{-C_2 p} - e^{-C_3 p}\right)(10\vartheta - 2) \\
&- C_4 \left(e^{-C_5 p} - e^{-C_6 p}\right)(10\vartheta - 1)
\end{aligned} \tag{41}$$

where ϑ is the thickness-to-length ratio and h/a and C_i are the corresponding constant coefficients, values of which are listed in Table 3. If you need more detailed information about the principle and reason of the new shear correction factor model, you can read [63].

3.1. Static Deflections. The first example considers the deformations of the isotropic plates under the action of a uniform pressure $p_0 = 1000$ Pa with various boundary conditions, i.e., CCCC, CFCF, CCCF, CSCS, SSSS and CSFF, and different action regions as $[(0,1),(0,1)]$, $[(0.1, 0.9),(0.1,0.9)]$, $[(0.2,0.8),(0.2,0.8)]$, $[(0.3,0.7),(0.3,0.7)]$, and $[(0.4,0.6),(0.4,0.6)]$, and the results are shown in Table 4. Also, the deformations of the isotropic plates with central point loading $p_0 = 0.1$ N are also considered in the Table 4. The locations of the maximum deflections obviously depend on the boundary condition, while the maximum deflection obviously occurs at the center of the clamped plate, but its locations will not be so clear for other boundary conditions. For comparison, the maximum deflections predicted by the ABAQUS based on the finite element method (FEM) are also given in Table 4 due to the lack of the reference data. Besides, the deflection fields of isotropic plate for the CCCC, CCCF, CFCF, and CSCF by means of the present method and finite element method are presented in Figure 3. The element type and mesh sizes of the ABAQUS model are the S4R and 0.01 m × 0.01 m, respectively. The geometrical parameters of the plate are defined as $a/b = 1$, $h/a = 0.05$, and $a = 1$ m, and the material parameter is chosen as the steel. From Table 4 and Figure 3, it is obvious

Table 2: The corresponding spring stiffness values for various boundary conditions.

Edges	Boundary condition	Essential conditions	Corresponding spring stiffness values		
			Γ_w	$\Gamma_{x,\text{or } y}$	Γ_{xy}
x = constant	Free (F)	$Q_x = M_x = M_{xy} = 0$	0	0	0
	Clamped (C)	$w = \varphi_x = \varphi_y = 0$	10^{15}	10^{15}	10^{15}
	Simply supported (S)	$w = M_x = \varphi_y = 0$	10^{15}	0	10^{15}
y = constant	Free (F)	$Q_x = M_y = M_{xy} = 0$	0	0	0
	Clamped (C)	$w = \varphi_y = \varphi_x = 0$	10^{15}	10^{15}	10^{15}
	Simply supported (S)	$w = M_y = \varphi_x$	10^{15}	0	10^{15}

Table 3: The values of the constant coefficients used in κ function for two FGMs.

FGMs	Constant coefficients					
	C_1	C_2	C_3	C_4	C_5	C_6
Al/Al_2O_3	0.750	0.025	2.000	0.640	0.060	1.000
Al/ZrO_2	0.560	0.001	5.450	0.420	0.095	1.175

that the present solution has excellent prediction accuracy for the static deflection.

Based on the verification, some new results of the static deflection of the FG plate with different boundary conditions and FGs type will been shown in the Tables 5–7. Table 5 shows the maximum deflection for Al/Al_2O_3 and Al/ZrO_2 plate having CCCC, CSCS, CFCF, and SSSS boundary cases under a central concentrated force $p_0 = 1$ N. Also, the maximum deflections of Al/Al_2O_3 and Al/ZrO_2 plate having different boundary conditions with the uniform pressure acting on entire rectangular area and part rectangular area $[(0.2, 0.8), (0.5, 1.5)]$ are, respectively, performed in Tables 6 and 7. The geometrical parameters of the above Tables are used as follows: $b/a = 2$, $h/a = 0.1$, and $a = 1$ m. From the above tables, we can see that the maximum deflection increases with the increase of the power-law exponent p, regardless of the boundary conditions and load functions. In order to complete this study and to further enhance the understanding of this phenomenon, the relations between the maximum deflection and power-law exponent p are shown in Figures 4 and 5. The geometrical parameters of those are the same as those of Tables 5–7. The variation of the static deflection versus the power-law exponent p for FG plate with central concentrated force subject to different boundary condition is presented in Figure 4. Two FG materials Al/Al_2O_3 and Al/ZrO_2 are considered in Figure 4. For the Al/Al_2O_3 plate, no matter what the boundary condition is, the maximum deflection keeps increasing when the power-law exponent p increases. However, for the Al/ZrO_2 plate, the maximum deflection trace climbs up, then declines, and reaches its crest around in the critical value. Figure 5 shows the variations of the static deflection versus the power-law exponent p for Al/Al_2O_3 plate having the uniform pressure with different acting regions which are the same as those of Tables 6 and 7. Four kinds boundary condition, i.e., CCCC, CSCS, CFCF, and SSSS, are considered. We can see clearly that the maximum deflection always climbs up versus the increase of the power-law exponent p regardless of the boundary condition and load type. Finally, those results in Tables 5–7 and Figures 4-5 may serve as the benchmark data of FG plate for the future works in this filed.

3.2. Free Vibration Analysis. In dynamic analysis like the steady state response and transient response, the free vibration plays an important role. Thus, in this subsection, our attention will be focused on the modal results. To start with, a verification study is given to display the accuracy and reliability of the current method. In Table 8, the present method is verified by comparing the evaluation of fundamental frequency parameters $\Omega = \omega h(\rho_m/E_m)^{1/2}$ for a simply supported Al/ZrO2 square plate with those of the finite element HSDT method [7], finite element FSDT method [7], two-dimensional higher-order theory [20], an analytical FSDT solution [63], an exact closed-form procedure on basis FSDT [22], and three-dimensional theory by employing the power series method [23]. From Table 8, it is not hard to see that the results obtained by the present method are in close agreement with those obtained by other methods. For the sake of completeness, the comparison for the fundamental frequency $\Omega = \omega h(\rho_c/E_c)^{1/2}$ of Al/Al_2O_3 and Al/ZrO_2 plates under six combinations of boundary conditions, i.e., SSSC, SCSC, SSSF, SCSF, and SFSF, is given in Tables 9 and 10, respectively. The results reported by Hashemi et al. [63] on the basis of the FSDT are included in the comparison. Although different solution approaches are used in the literature, it is still clearly seen that the present results and referential data agree well with each other.

After the verification, some new vibration results of FG plate with a variety of boundary conditions will be obtained in Tables 11 and 12 by using the present solution. In cases of Table 11, the FG plates are fabricated from aluminum (metal) and alumina (ceramic). In cases of Table 12, the FG plates are fabricated from aluminum (metal) and zirconia (ceramic). The geometrical parameters and power-law exponents of the FG plate are taken to be $b/a = 2$, $h/a = 0.05$, 0.1, and 0.2, and $p = 0$, 0.5, 1, 5, and 10. Some selected mode shapes of the Al/Al_2O_3 plate are as shown in Figure 6. From Tables 11-12, the power-law exponent significantly affects the

Table 4: Comparison of the maximum deflection for isotropic square plates having various boundary conditions with different load functions.

Boundary conditions	Method	Uniform pressure					Point Load: (0.5, 0.5)
		[(0, 1), (0, 1)]	[(0.1, 0.9), (0.1, 0.9)]	[(0.2, 0.8), (0.2, 0.8)]	[(0.3, 0.7), (0.3, 0.7)]	[(0.4, 0.6), (0.4, 0.6)]	
CCCC	Present	5.602E-07	5.438E-07	4.530E-07	2.790E-07	8.901E-08	2.522E-10
	FEM	5.602E-07	5.438E-07	4.530E-07	2.789E-07	8.896E-08	2.563E-10
CFCF	Present	1.278E-06	9.716E-07	7.275E-07	4.116E-07	1.237E-07	3.401E-10
	FEM	1.278E-06	9.716E-07	7.273E-07	4.115E-07	1.236E-07	3.431E-10
CCCF	Present	1.301E-09	8.452E-07	6.152E-07	3.502E-07	1.066E-07	2.950E-10
	FEM	1.302E-09	8.452E-07	6.150E-07	3.501E-07	1.065E-07	2.981E-10
CSCS	Present	8.406E-07	7.930E-07	6.272E-07	3.677E-07	1.129E-07	3.157E-10
	FEM	8.406E-07	7.930E-07	6.272E-07	3.677E-07	1.129E-07	3.174E-10
SSSS	Present	1.737E-06	1.584E-06	1.175E-06	6.448E-07	1.874E-07	5.064E-10
	FEM	1.737E-06	1.585E-06	1.740E-06	6.447E-07	1.873E-07	5.076E-10
CSFF	Present	3.084E-05	1.858E-05	9.955E-06	4.267E-06	1.043E-06	2.604E-09
	FEM	3.084E-05	1.858E-05	9.955E-06	4.267E-06	1.043E-06	2.618E-09

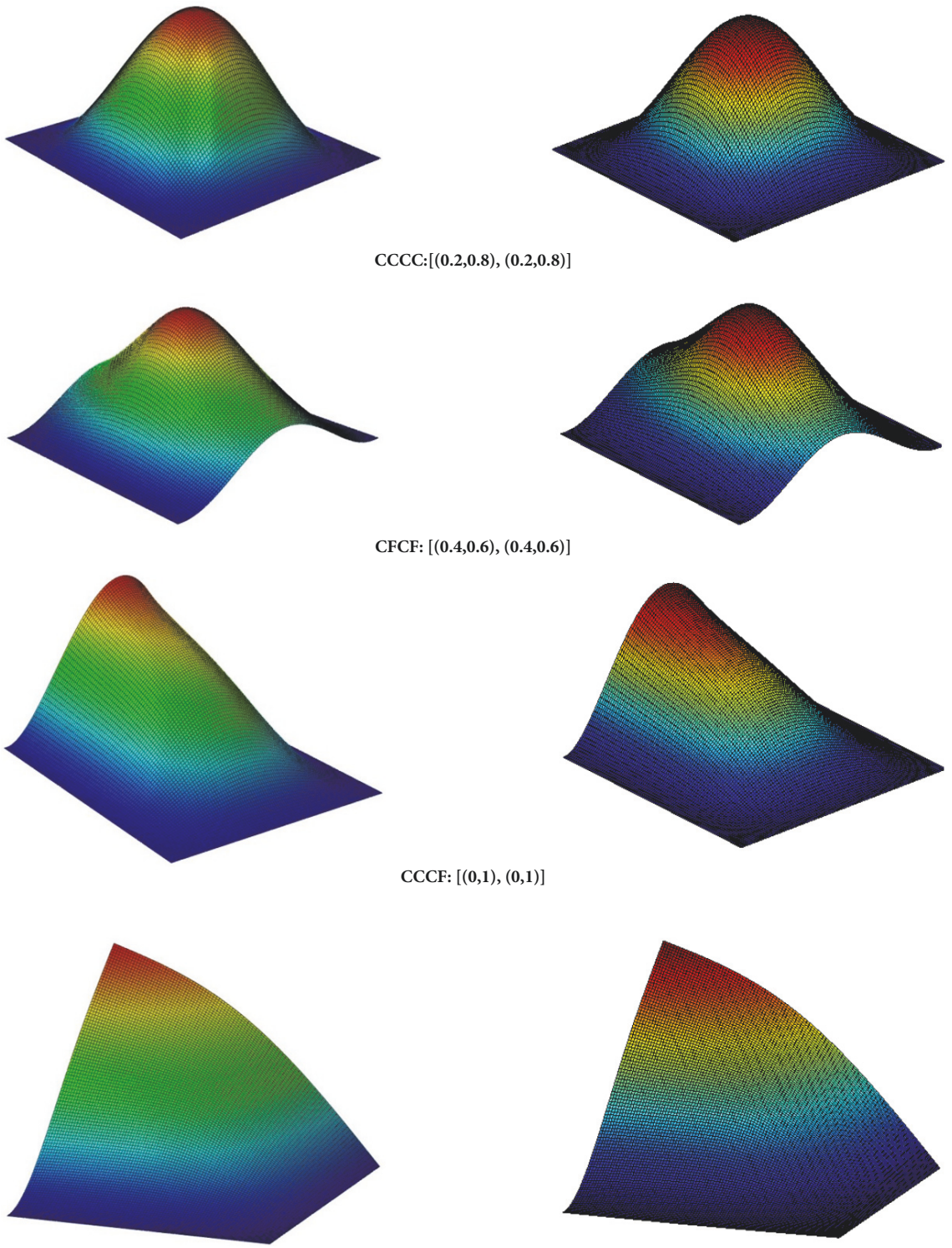

Figure 3: Static deflection of an isotropic plate under different loads: (a) finite element (ABAQUS); (b) current solution.

Table 5: Maximum deflection W for FG plates having various boundary conditions with the central point load.

p	Al/Al_2O_3				Al/ZrO_2			
	CCCC	CSCS	CFCF	SSSS	CCCC	CSCS	CFCF	SSSS
0	2.542E-10	4.867E-10	1.349E-09	5.183E-10	4.830E-10	9.248E-10	2.564E-09	9.847E-10
0.5	4.429E-10	7.747E-10	2.051E-09	8.179E-10	8.237E-10	1.402E-09	3.657E-09	1.477E-09
2	1.040E-09	1.486E-09	3.442E-09	1.536E-09	1.123E-09	1.840E-09	4.683E-09	1.928E-09
5	1.201E-09	1.746E-09	4.100E-09	1.806E-09	1.322E-09	2.138E-09	5.400E-09	2.234E-09
10	1.205E-09	1.873E-09	4.621E-09	1.952E-09	1.472E-09	2.390E-09	6.048E-09	2.498E-09
50	1.223E-09	2.236E-09	6.065E-09	2.371E-09	1.701E-09	2.841E-09	7.304E-09	2.982E-09
100	1.264E-09	2.381E-09	6.557E-09	2.532E-09	1.709E-09	2.896E-09	7.539E-09	3.049E-09

Table 6: Maximum deflection W for FG plates having various boundary conditions with the uniform pressure in the entire rectangular area.

p	Al/Al_2O_3				Al/ZrO_2			
	CCCC	CSCS	CFCF	SSSS	CCCC	CSCS	CFCF	SSSS
0	8.316E-08	2.543E-07	1.355E-06	3.004E-07	1.580E-07	4.832E-07	2.575E-06	5.708E-07
0.5	1.363E-07	3.837E-07	2.021E-06	4.467E-07	2.490E-07	6.818E-07	3.576E-06	7.899E-07
2	2.800E-07	6.243E-07	3.167E-06	6.980E-07	3.306E-07	8.706E-07	4.538E-06	1.002E-06
5	3.274E-07	7.476E-07	3.808E-06	8.393E-07	3.857E-07	1.001E-06	5.207E-06	1.149E-06
10	3.429E-07	8.496E-07	4.385E-06	9.672E-07	4.312E-07	1.122E-06	5.838E-06	1.288E-06
50	3.878E-07	1.139E-06	6.036E-06	1.336E-06	5.072E-07	1.361E-06	7.113E-06	1.571E-06
100	4.089E-07	1.235E-06	6.569E-06	1.455E-06	5.145E-07	1.405E-06	7.368E-06	1.627E-06

Table 7: Maximum deflection for FG plates having various boundary conditions with the uniform pressure in the part rectangular area $[(0.2, 0.8), (0.5, 1.5)]$.

p	Al/Al_2O_3				Al/ZrO_2			
	CCCC	CSCS	CFCF	SSSS	CCCC	CSCS	CFCF	SSSS
0	6.583E-08	1.713E-07	6.209E-07	1.897E-07	1.251E-07	3.254E-07	1.180E-06	3.604E-07
0.5	1.072E-07	2.583E-07	9.251E-07	2.834E-07	1.954E-07	4.590E-07	1.637E-06	5.021E-07
2	2.160E-07	4.213E-07	1.452E-06	4.507E-07	2.585E-07	5.861E-07	2.078E-06	6.384E-07
5	2.530E-07	5.043E-07	1.745E-06	5.408E-07	3.012E-07	6.742E-07	2.384E-06	7.333E-07
10	2.669E-07	5.723E-07	2.009E-06	6.192E-07	3.369E-07	7.555E-07	2.673E-06	8.219E-07
50	3.060E-07	7.668E-07	2.764E-06	8.454E-07	3.972E-07	9.160E-07	3.257E-06	9.999E-07
100	3.233E-07	8.314E-07	3.009E-06	9.193E-07	4.035E-07	9.461E-07	3.373E-06	1.035E-06

fundamental frequency of the FG plate. To have a more intuitive understanding, the variation of the fundamental frequencies of FG plate with power-law exponents and different boundary conditions is depicted in Figures 7-8. From Figure 7, we can see that the fundamental frequencies decrease monotonously while increasing the power-law index p. Moreover, the fundamental frequencies rapidly decrease, then increase, and finally decrease with the power-law index p increasing, when the FG plate is fabricated from aluminum (metal) and zirconia (ceramic).

4. Conclusions

This paper presents a unified functionally graded Reissner-Mindlin rectangular plate model with general boundary conditions for static and vibration analysis. The unified model is based on the Reissner-Mindlin plate theory and the general boundary condition is implemented by using the arbitrary boundary technique which consists of one group of liner spring and two groups of rotation springs along all edges. An improved Fourier series method which contains a 2D Fourier cosine series and auxiliary function in the form of 1D series is introduced to formulate the components of admissible displacement functions. The target of the auxiliary function is to remove the potential discontinuities of the displacement function and their derivative at the edges, and ensure and accelerate the convergence of the series representation. This solution method is exact in the sense that the governing differential equation and the boundary conditions are simultaneously satisfied, on a point-wise basis, to any specified accuracy. The excellent accuracy and reliability of the present method are displayed by comparing its static and vibration predictions with those of other techniques. The research of static and vibration analysis of FG plate could provide the theoretical basis for practical engineering applications. And the results of this paper could serve as the reference data in practical engineering applications in related field in future.

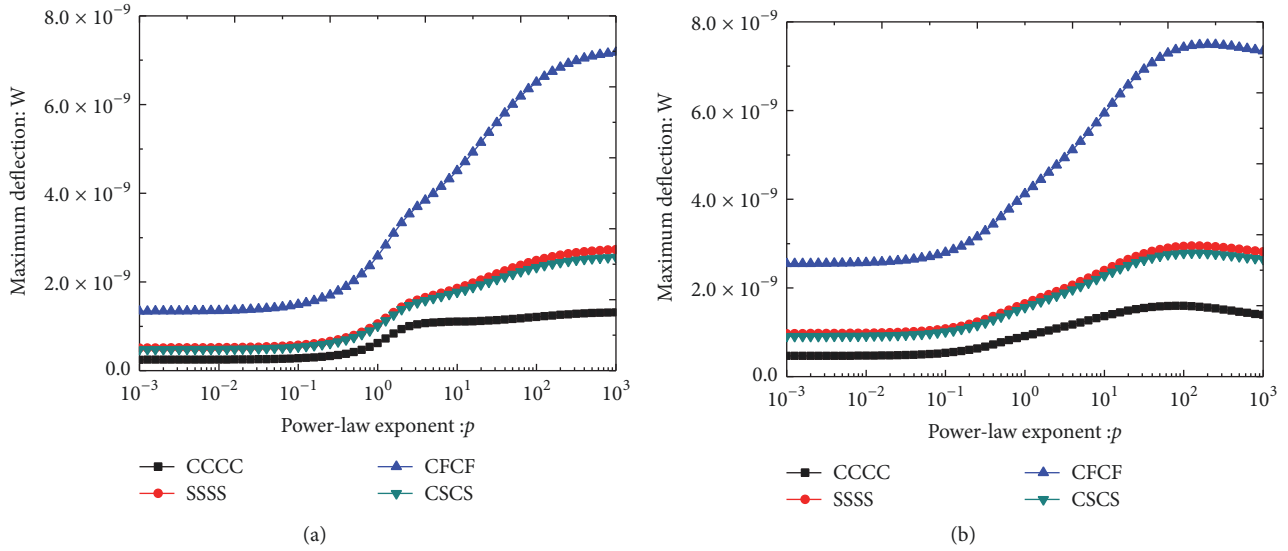

Figure 4: Variation of the static deflection versus the power-law exponent p for FG plate with central point load: (a) Al/Al_2O_3 plate; (b) Al/ZrO_2 plate.

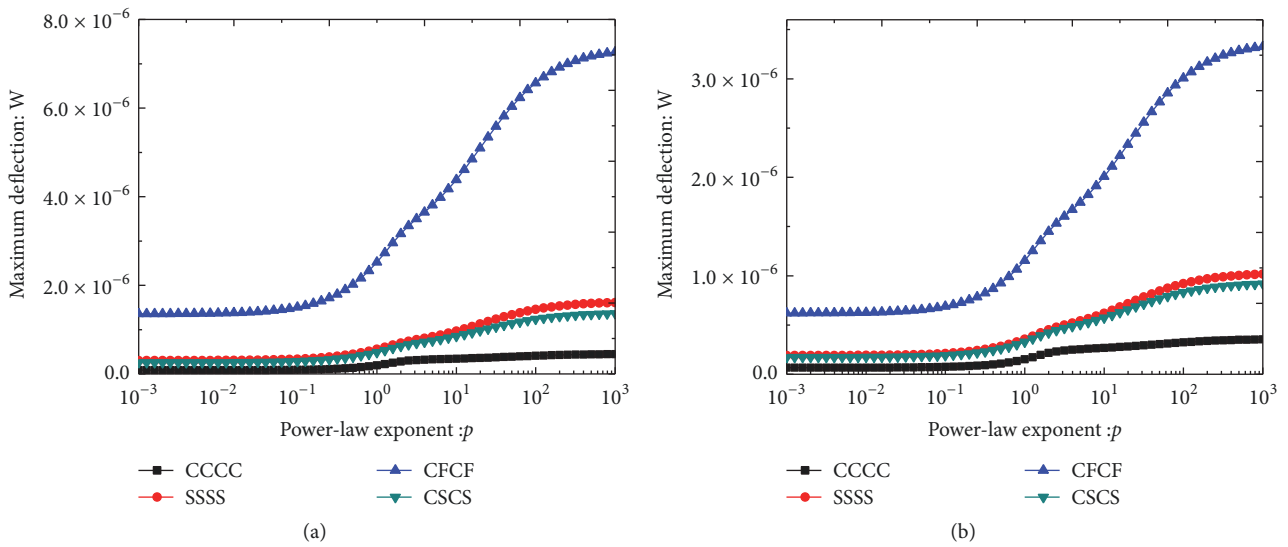

Figure 5: Variation of the static deflection versus the power-law exponent p for Al/Al_2O_3 plate with different uniform press: (a) entire rectangular plate; (b) part rectangular area $[(0.2, 0.8), (0.5, 1.5)]$.

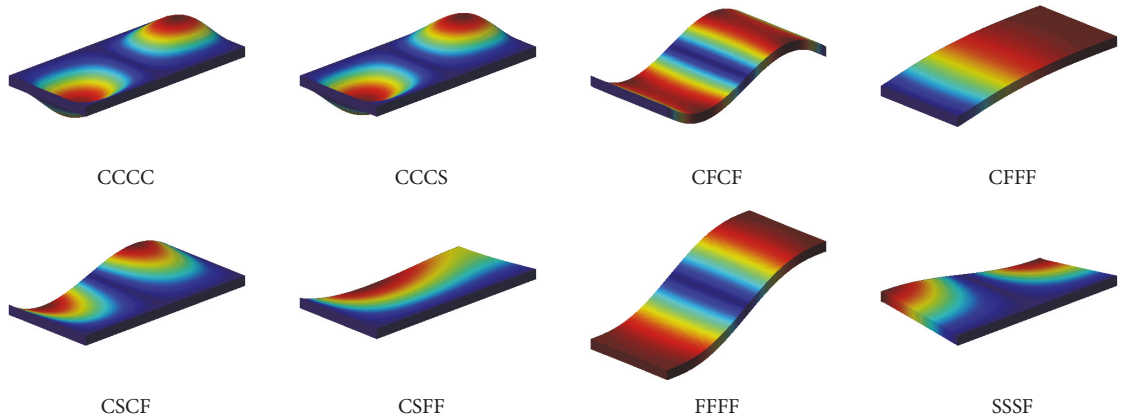

Figure 6: Fundamental mode shape of Al/Al_2O_3 plates with different boundary conditions.

Table 8: Comparison of fundamental frequency parameter $\Omega = \omega h(\rho_m/E_m)^{1/2}$ for SSSS Al/ZrO_2 square plates. Table 8 is reproduced from Wang [42] et al. (2017) (under the Creative Commons Attribution License/public domain).

Method	$p = \infty$			$p = 1$		$h/a = 0.2$		
	$h/a = 1/\sqrt{10}$	$h/a = 0.1$	$h/a = 0.05$	$h/a = 0.1$	$h/a = 0.2$	$p = 2$	$p = 3$	$p = 5$
present	0.4618	0.0577	0.0159	0.0611	0.2270	0.2249	0.2254	0.2265
HSDT [7]	0.4658	0.0578	0.0157	0.0613	0.2257	0.2237	0.2243	0.2253
FSDT [7]	0.4619	0.0577	0.0162	0.0633	0.2323	0.2325	0.2334	0.2334
HSDT [20]	0.4658	0.0577	0.0158	0.0619	0.2285	0.2264	0.2270	0.2281
FSDT [23]	0.4618	0.0576	0.0158	0.0611	0.227	0.2249	0.2254	0.2265
FSDT [24]	0.4618	0.0577	0.0158	0.0619	0.2276	0.2264	0.2276	0.2291
3-D [27]	0.4658	0.0577	0.0153	0.0596	0.2192	0.2197	0.2211	0.2225

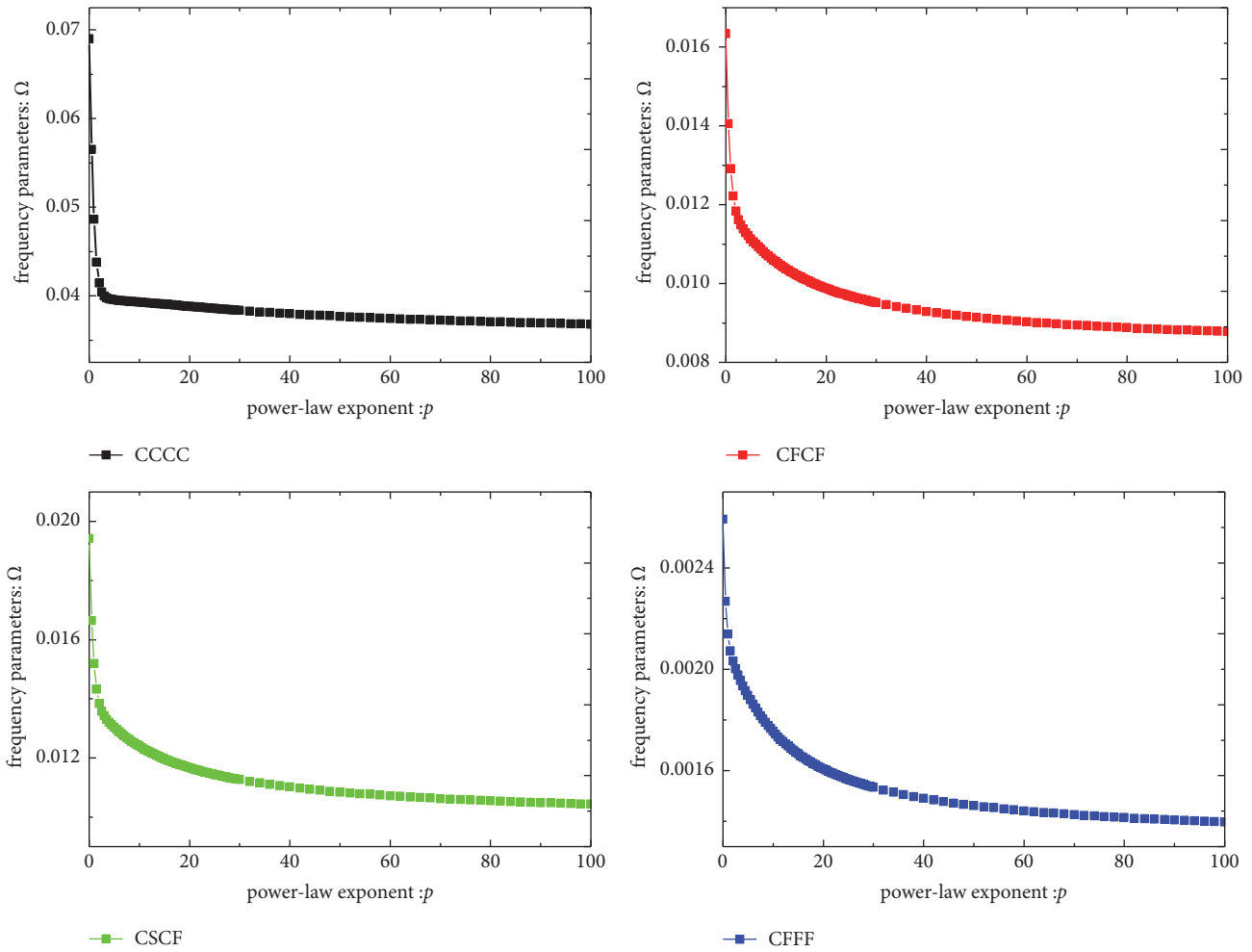

Figure 7: Variations of fundamental frequency parameter Ω versus the power-law exponent p for Al/Al_2O_3 rectangular plate with different boundary conditions.

Data Availability

The data used to support the findings of this study are available from the corresponding author upon request.

Conflicts of Interest

The authors declare that they have no conflicts of interest.

Acknowledgments

This study was funded by High Technology Ship Funds of Ministry of Industry and Information of China, Ph.D. Student Research and Innovation Fund of the Fundamental Research Funds for the Central Universities (HEUGIP201801), Assembly Advanced Research Fund of China (6140210020105), Major Innovation Projects of

Table 9: Comparison of fundamental frequency parameter $\Omega = \omega h(\rho_c/E_c)^{1/2}$ for Al/Al_2O_3 plates when $h/a = 0.15$.

b/a	p	SSSC		SCSC		SSSF		SFSF		SCSF	
		Exact	Present	Exact	Present	Exact	Present	Exact	Present	Exact	Present
2	0	0.08325	0.08325	0.08729	0.08729	0.06713	0.06713	0.06364	0.06365	0.06781	0.06781
	0.25	0.07600	0.07600	0.07950	0.07950	0.06145	0.06145	0.05829	0.05829	0.06205	0.06205
	1	0.06541	0.06541	0.06790	0.06790	0.05346	0.05346	0.05080	0.05080	0.05391	0.05391
	5	0.05524	0.05524	0.05695	0.05695	0.04568	0.04568	0.04349	0.04349	0.04600	0.04600
	∞	0.04263	0.04237	0.04443	0.04443	0.03417	0.03417	0.03239	0.03240	0.03451	0.03452
1	0	0.14378	0.14377	0.16713	0.16712	0.07537	0.07537	0.06290	0.06290	0.08062	0.08062
	0.25	0.12974	0.12973	0.14927	0.14926	0.06890	0.06890	0.05761	0.05761	0.07351	0.07350
	1	0.10725	0.10725	0.11955	0.11955	0.05968	0.05968	0.05021	0.05021	0.06308	0.06308
	5	0.08720	0.08720	0.09479	0.09479	0.05078	0.05078	0.04301	0.04300	0.05322	0.05322
	∞	0.07318	0.07318	0.08507	0.08507	0.03836	0.03836	0.03202	0.03202	0.04104	0.04104
0.5	0	0.35045	0.35037	0.41996	0.41980	0.10065	0.10065	0.06217	0.06216	0.13484	0.13483
	0.25	0.30709	0.30703	0.36112	0.36102	0.09170	0.09170	0.05695	0.05695	0.12160	0.12159
	1	0.23262	0.23260	0.26091	0.26088	0.07851	0.07851	0.04970	0.04970	0.10066	0.10066
	5	0.17691	0.17690	0.19258	0.19257	0.06610	0.06610	0.04262	0.04262	0.08226	0.08226
	∞	0.17921	0.17837	0.21375	0.21374	0.05123	0.05123	0.03164	0.03164	0.06863	0.06863

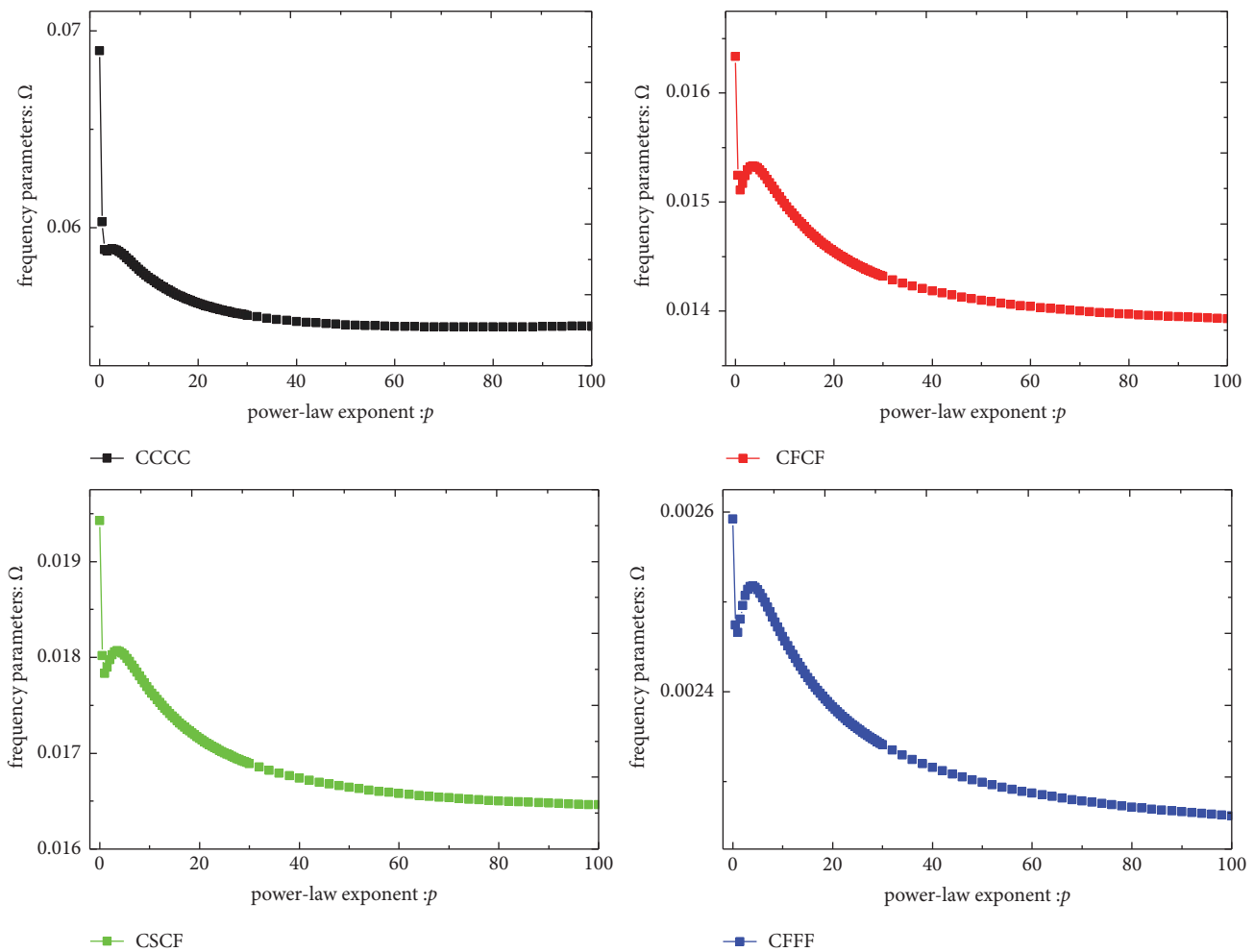

Figure 8: Variations of fundamental frequency parameter Ω versus the power-law exponent p for Al/ZrO_2 rectangular plate with different boundary conditions.

Table 10: Comparison of fundamental frequency parameter $\Omega = \omega h(\rho_c/E_c)^{1/2}$ for Al/ZrO_2 plates when $a/b = 1.5$.

h/a	p	SSSC		SCSC		SSSF		SFSF		SCSF	
		Exact	Present	Exact	Present	Exact	Present	Exact	Present	Exact	Present
0.05	0	0.03129	0.03130	0.04076	0.04076	0.01024	0.01024	0.00719	0.00719	0.01249	0.012492
	0.25	0.02899	0.02899	0.03664	0.03664	0.00981	0.00981	0.00692	0.00692	0.01185	0.011851
	1	0.02667	0.02667	0.03250	0.03250	0.00948	0.00948	0.00674	0.00674	0.01132	0.011316
	5	0.02677	0.02677	0.03239	0.03239	0.00963	0.00963	0.00685	0.00685	0.01146	0.01146
	∞	0.02689	0.02689	0.03502	0.03502	0.00880	0.00880	0.00618	0.00618	0.01073	0.010734
0.1	0	0.11639	0.11638	0.14580	0.14580	0.04001	0.04001	0.02835	0.02835	0.04817	0.04817
	0.25	0.10561	0.10561	0.12781	0.12780	0.03810	0.03810	0.02717	0.02717	0.04532	0.045315
	1	0.09734	0.09733	0.11453	0.11453	0.03679	0.03679	0.02641	0.02641	0.04327	0.043267
	5	0.09646	0.09646	0.11234	0.11234	0.03718	0.03718	0.02677	0.02677	0.04352	0.043517
	∞	0.10001	0.10001	0.12528	0.12528	0.03438	0.03438	0.02426	0.02436	0.04139	0.041391
0.2	0	0.37876	0.37870	0.43939	0.43930	0.14871	0.14871	0.10795	0.10795	0.17323	0.173218
	0.25	0.36117	0.36113	0.41624	0.41617	0.14354	0.14354	0.10436	0.10436	0.16671	0.1667
	1	0.33549	0.33547	0.37962	0.37958	0.13851	0.13851	0.10127	0.10127	0.15937	0.159366
	5	0.32783	0.32781	0.36695	0.36692	0.13888	0.13887	0.10200	0.10200	0.15878	0.158779
	∞	0.32545	0.32544	0.37755	0.37753	0.12779	0.12778	0.09276	0.09276	0.14885	0.148845

Table 11: Fundamental frequency parameter $\Omega = \omega h(\rho_c/E_c)^{1/2}$ for Al/Al_2O_3 plates with different boundary conditions.

h/a	p	Boundary conditions							
		CCCC	CCCS	CFCF	FFFF	CSCF	CSFF	CFFF	SSSF
0.05	0	0.01822	0.01370	0.00414	0.00405	0.00495	0.00160	0.00065	0.00303
	0.5	0.01541	0.01175	0.00360	0.00355	0.00429	0.00139	0.00057	0.00264
	1	0.01291	0.01027	0.00329	0.00333	0.00389	0.00129	0.00054	0.00246
	5	0.01111	0.00893	0.00290	0.00296	0.00342	0.00114	0.00048	0.00218
	10	0.01107	0.00868	0.00274	0.00274	0.00324	0.00107	0.00044	0.00203
0.1	0	0.06897	0.18772	0.01632	0.01608	0.01941	0.00630	0.00259	0.01200
	0.5	0.05652	0.15857	0.01406	0.01405	0.01663	0.00547	0.00227	0.01043
	1	0.04862	0.14291	0.01291	0.01320	0.01519	0.00509	0.00214	0.00974
	5	0.03953	0.11409	0.01113	0.01166	0.01303	0.00446	0.00190	0.00856
	10	0.03929	0.11157	0.01054	0.01082	0.01239	0.00417	0.00175	0.00798
0.2	0	0.23286	0.18772	0.06198	0.06260	0.07269	0.02439	0.01026	0.04657
	0.5	0.19360	0.15857	0.05338	0.05472	0.06242	0.02121	0.00899	0.04055
	1	0.17136	0.14291	0.04927	0.05147	0.05740	0.01983	0.00848	0.03798
	5	0.13242	0.11409	0.04126	0.04505	0.04776	0.01714	0.00749	0.03295
	10	0.13167	0.11157	0.03935	0.04191	0.04569	0.01606	0.00694	0.03081

Table 12: Fundamental frequency parameter $\Omega = \omega h(\rho_c/E_c)^{1/2}$ for Al/ZrO_2 plates with different boundary conditions.

h/a	p	Boundary conditions							
		CCCC	CCCS	CFCF	FFFF	CSCF	CSFF	CFFF	SSSF
0.05	0	0.01822	0.01370	0.00414	0.00405	0.00495	0.00160	0.00065	0.00303
	0.5	0.01606	0.01246	0.00388	0.00386	0.00461	0.00150	0.00062	0.00287
	1	0.01588	0.01235	0.00386	0.00385	0.00458	0.00150	0.00062	0.00286
	5	0.01598	0.01249	0.00393	0.00392	0.00465	0.00153	0.00063	0.00291
	10	0.01481	0.01179	0.00378	0.00383	0.00447	0.00148	0.00062	0.00283
0.1	0	0.06897	0.05286	0.01632	0.01608	0.01941	0.00630	0.00259	0.01200
	0.5	0.06029	0.04770	0.01524	0.01532	0.01801	0.00595	0.00247	0.01135
	1	0.05888	0.04690	0.01511	0.01526	0.01782	0.00591	0.00246	0.01129
	5	0.05858	0.04702	0.01529	0.01553	0.01801	0.00601	0.00251	0.01148
	10	0.05748	0.04611	0.01498	0.01521	0.01765	0.00588	0.00246	0.01124
0.2	0	0.23288	0.18773	0.06198	0.06260	0.07269	0.02439	0.01026	0.04657
	0.5	0.21550	0.17558	0.05870	0.05988	0.06871	0.02324	0.00983	0.04442
	1	0.20752	0.17074	0.05782	0.05952	0.06754	0.02304	0.00979	0.04407
	5	0.20352	0.16912	0.05810	0.06038	0.06770	0.02332	0.00996	0.04464
	10	0.20672	0.17013	0.05770	0.05935	0.06737	0.02300	0.00978	0.04398

High Technology Ship Funds of Ministry of Industry and Information of China, National key Research and Development Program (2016YFC0303406), Naval Pre-Research Project, Fundamental Research Funds for the Central University (HEUCFD1515, HEUCFM170113), China Postdoctoral Science Foundation (2014M552661), and National Natural Science Foundation of China (51209052, 51709063).

References

[1] M. Koizumi, "FGM activities in Japan," *Composites Part B: Engineering*, vol. 28, no. 1-2, pp. 1–4, 1997.

[2] C. T. Loy, K. Y. Lam, and J. N. Reddy, "Vibration of functionally graded cylindrical shells," *International Journal of Mechanical Sciences*, vol. 41, no. 3, pp. 309–324, 1999.

[3] S. Abrate, "Functionally graded plates behave like homogeneous plates," *Composites Part B: Engineering*, vol. 39, no. 1, pp. 151–158, 2008.

[4] S. Abrate, "Free vibration, buckling, and static deflections of functionally graded plates," *Composites Science and Technology*, vol. 66, no. 14, pp. 2383–2394, 2006.

[5] L. F. Qian, R. C. Batra, and L. M. Chen, "Free and forced vibrations of thick rectangular plates using higher-order shear and normal deformable plate theory and Meshless Petrov-Galerkin (MLPG) method," *Computer Modeling in Engineering and Sciences*, vol. 4, no. 5, pp. 519–534, 2003.

[6] L. F. Qian, R. C. Batra, and L. M. Chen, "Static and dynamic deformations of thick functionally graded elastic plates by using higher order shear and normal deformable plate theory and meshless local Petrov-Galerkin method," *Composites Part B: Engineering*, vol. 35, no. 6–8, pp. 685–697, 2004.

[7] S. Pradyumna and J. N. Bandyopadhyay, "Free vibration analysis of functionally graded curved panels using a higher-order finite element formulation," *Journal of Sound and Vibration*, vol. 318, no. 1-2, pp. 176–192, 2008.

[8] A. J. M. Ferreira, R. C. Batra, C. M. C. Roque, L. F. Qian, and R. M. N. Jorge, "Natural frequencies of functionally graded plates by a meshless method," *Composite Structures*, vol. 75, no. 1-4, pp. 593–600, 2006.

[9] G. N. Praveen and J. N. Reddy, "Nonlinear transient thermoelastic analysis of functionally graded ceramic-metal plates," *International Journal of Solids and Structures*, vol. 35, no. 33, pp. 4457–4476, 1998.

[10] J. N. Reddy, "Analysis of functionally graded plates," *International Journal for Numerical Methods in Engineering*, vol. 47, no. 1–3, pp. 663–684, 2000.

[11] L. Della Croce and P. Venini, "Finite elements for functionally graded Reissner-Mindlin plates," *Computer Methods Applied Mechanics and Engineering*, vol. 193, no. 9-11, pp. 705–725, 2004.

[12] Z.-Q. Cheng and R. C. Batra, "Deflection relationships between the homogeneous Kirchhoff plate theory and different functionally graded plate theories," *Archives of Mechanics*, vol. 52, no. 1, pp. 143–158, 2000.

[13] Z.-Q. Cheng and R. C. Batra, "Exact correspondence between eigenvalues of membranes and functionally graded simply supported polygonal plates," *Journal of Sound and Vibration*, vol. 229, no. 4, pp. 879–895, 2000.

[14] X. Zhao, Y. Y. Lee, and K. M. Liew, "Free vibration analysis of functionally graded plates using the element-free kp-Ritz method," *Journal of Sound and Vibration*, vol. 319, no. 3–5, pp. 918–939, 2009.

[15] J. Woo, S. A. Meguid, and L. S. Ong, "Nonlinear free vibration behavior of functionally graded plates," *Journal of Sound and Vibration*, vol. 289, no. 3, pp. 595–611, 2006.

[16] J. Yang and H.-S. Shen, "Dynamic response of initially stressed functionally graded rectangular thin plates," *Composite Structures*, vol. 54, no. 4, pp. 497–508, 2001.

[17] J. Yang and H.-S. Shen, "Vibration characteristics and transient response of shear-deformable functionally graded plates in thermal environments," *Journal of Sound and Vibration*, vol. 255, no. 3, pp. 579–602, 2002.

[18] Z. Zhong and T. Yu, "Vibration of a simply supported functionally graded piezoelectric rectangular plate," *Smart Materials and Structures*, vol. 15, no. 5, article no. 029, pp. 1404–1412, 2006.

[19] C. M. C. Roque, A. J. M. Ferreira, and R. M. N. Jorge, "A radial basis function approach for the free vibration analysis of functionally graded plates using a refined theory," *Journal of Sound and Vibration*, vol. 300, no. 3-5, pp. 1048–1070, 2007.

[20] H. Matsunaga, "Free vibration and stability of functionally graded plates according to a 2-D higher-order deformation theory," *Composite Structures*, vol. 82, no. 4, pp. 499–512, 2008.

[21] P. Yousefi, M. H. Kargarnovin, and S. H. Hosseini-Hashemi, "Free vibration of generally laminated plates with various shapes," *Polymer Composites*, vol. 32, no. 3, pp. 445–454, 2011.

[22] S. Hosseini-Hashemi, M. Fadaee, and S. R. Atashipour, "A new exact analytical approach for free vibration of Reissner–Mindlin functionally graded rectangular plates," *International Journal of Mechanical Sciences*, vol. 53, no. 1, pp. 11–22, 2011.

[23] S. S. Vel and R. C. Batra, "Three-dimensional exact solution for the vibration of functionally graded rectangular plates," *Journal of Sound and Vibration*, vol. 272, no. 3–5, pp. 703–730, 2004.

[24] S. M. Shiyekar and T. Kant, "An electromechanical higher order model for piezoelectric functionally graded plates," *International Journal of Mechanics and Materials in Design*, vol. 6, no. 2, pp. 163–174, 2010.

[25] E. Carrera, S. Brischetto, M. Cinefra, and M. Soave, "Effects of thickness stretching in functionally graded plates and shells," *Composites Part B: Engineering*, vol. 42, no. 2, pp. 123–133, 2011.

[26] A. M. A. Neves, A. J. M. Ferreira, E. Carrera et al., "Static, free vibration and buckling analysis of isotropic and sandwich functionally graded plates using a quasi-3D higher-order shear deformation theory and a meshless technique," *Composites Part B: Engineering*, vol. 44, no. 1, pp. 657–674, 2013.

[27] L. W. Zhang, P. Zhu, and K. M. Liew, "Thermal buckling of functionally graded plates using a local Kriging meshless method," *Composite Structures*, vol. 108, pp. 472–492, 2014.

[28] Z. Belabed, M. S. A. Houari, A. Tounsi, S. R. Mahmoud, and O. Anwar Bég, "An efficient and simple higher order shear and normal deformation theory for functionally graded material (FGM) plates," *Composites Part B: Engineering*, vol. 60, pp. 274–283, 2014.

[29] H.-T. Thai and D.-H. Choi, "A refined shear deformation theory for free vibration of functionally graded plates on elastic foundation," *Composites Part B: Engineering*, vol. 43, no. 5, pp. 2335–2347, 2012.

[30] H.-T. Thai and D.-H. Choi, "A simple first-order shear deformation theory for the bending and free vibration analysis of functionally graded plates," *Composite Structures*, vol. 101, pp. 332–340, 2013.

[31] H.-T. Thai and S.-E. Kim, "A simple higher-order shear deformation theory for bending and free vibration analysis of functionally graded plates," *Composite Structures*, vol. 96, pp. 165–173, 2013.

[32] H.-T. Thai and S.-E. Kim, "A simple quasi-3D sinusoidal shear deformation theory for functionally graded plates," *Composite Structures*, vol. 99, pp. 172–180, 2013.

[33] H.-T. Thai and S.-E. Kim, "Closed-form solution for buckling analysis of thick functionally graded plates on elastic foundation," *International Journal of Mechanical Sciences*, vol. 75, pp. 34–44, 2013.

[34] H.-T. Thai and T. P. Vo, "A new sinusoidal shear deformation theory for bending, buckling, and vibration of functionally graded plates," *Applied Mathematical Modelling: Simulation and Computation for Engineering and Environmental Systems*, vol. 37, no. 5, pp. 3269–3281, 2013.

[35] N. Valizadeh, S. Natarajan, O. A. Gonzalez-Estrada, T. Rabczuk, T. Q. Bui, and S. P. A. Bordas, "NURBS-based finite element analysis of functionally graded plates: Static bending, vibration, buckling and flutter," *Composite Structures*, vol. 99, pp. 309–326, 2013.

[36] L. V. Tran, A. J. M. Ferreira, and H. Nguyen-Xuan, "Isogeometric analysis of functionally graded plates using higher-order shear deformation theory," *Composites Part B: Engineering*, vol. 51, no. 4, pp. 368–383, 2013.

[37] J. L. Mantari and C. Guedes Soares, "A novel higher-order shear deformation theory with stretching effect for functionally graded plates," *Composites Part B: Engineering*, vol. 45, no. 1, pp. 268–281, 2013.

[38] S. Xiang and G.-w. Kang, "A *n*th-order shear deformation theory for the bending analysis on the functionally graded plates," *European Journal of Mechanics - A/Solids*, vol. 37, pp. 336–343, 2013.

[39] N. Fantuzzi, F. Tornabene, and E. Viola, "Four-parameter functionally graded cracked plates of arbitrary shape: a GDQFEM solution for free vibrations," *Mechanics of Advanced Materials and Structures*, vol. 23, no. 1, pp. 89–107, 2016.

[40] H. Nguyen-Xuan, L. V. Tran, C. H. Thai, S. Kulasegaram, and S. P. A. Bordas, "Isogeometric analysis of functionally graded plates using a refined plate theory," *Composites Part B: Engineering*, vol. 64, pp. 222–234, 2014.

[41] S. S. Akavci, "An efficient shear deformation theory for free vibration of functionally graded thick rectangular plates on elastic foundation," *Composite Structures*, vol. 108, no. 1, pp. 667–676, 2014.

[42] Q. Wang, D. Shi, Q. Liang, and F. Pang, "A unified solution for vibration analysis of moderately thick, functionally graded rectangular plates with general boundary restraints and internal line supports," *Mechanics of Advanced Materials and Structures*, vol. 24, no. 11, pp. 961–973, 2017.

[43] F. Pang et al., "A semi analytical method for the free vibration of doubly-curved shells of revolution," *Computers & Mathematics with Applications*, vol. 75, no. 9, pp. 3249–3268, 2018.

[44] F. Pang, H. Li, X. Miao, and X. Wang, "A modified Fourier solution for vibration analysis of moderately thick laminated annular sector plates with general boundary conditions, internal radial line and circumferential arc supports," *Curved and Layered Structures*, vol. 4, no. 1, 2017.

[45] F. Pang, H. Li, K. Choe, D. Shi, and K. Kim, "Free and Forced Vibration Analysis of Airtight Cylindrical Vessels with Doubly Curved Shells of Revolution by Using Jacobi-Ritz Method," *Shock and Vibration*, vol. 2017, pp. 1–20, 2017.

[46] Q. Wang, D. Shao, and B. Qin, "A simple first-order shear deformation shell theory for vibration analysis of composite laminated open cylindrical shells with general boundary conditions," *Composite Structures*, vol. 184, pp. 211–232, 2018.

[47] Q. Wang, K. Choe, D. Shi, and K. Sin, "Vibration analysis of the coupled doubly-curved revolution shell structures by using Jacobi-Ritz method," *International Journal of Mechanical Sciences*, vol. 135, pp. 517–531, 2018.

[48] Z. Su, G. Jin, Y. Wang, and X. Ye, "A general Fourier formulation for vibration analysis of functionally graded sandwich beams with arbitrary boundary condition and resting on elastic foundations," *Acta Mechanica*, vol. 227, no. 5, pp. 1493–1514, 2016.

[49] H. Khov, W. L. Li, and R. F. Gibson, "An accurate solution method for the static and dynamic deflections of orthotropic plates with general boundary conditions," *Composite Structures*, vol. 90, no. 4, pp. 474–481, 2009.

[50] W. L. Li, "Free vibrations of beams with general boundary conditions," *Journal of Sound and Vibration*, vol. 237, no. 4, pp. 709–725, 2000.

[51] G. Jin, T. Ye, X. Wang, and X. Miao, "A unified solution for the vibration analysis of FGM doubly-curved shells of revolution with arbitrary boundary conditions," *Composites Part B: Engineering*, vol. 89, pp. 230–252, 2016.

[52] L. Li, H. Li, F. Pang, X. Wang, Y. Du, and S. Li, "The modified Fourier-Ritz approach for the free vibration of functionally graded cylindrical, conical, spherical panels and shells of revolution with general boundary condition," *Mathematical Problems in Engineering*, Art. ID 9183924, 32 pages, 2017.

[53] H. Li, F. Pang, X. Wang, and S. Li, "Benchmark Solution for Free Vibration of Moderately Thick Functionally Graded Sandwich Sector Plates on Two-Parameter Elastic Foundation with General Boundary Conditions," *Shock and Vibration*, vol. 2017, Article ID 4018629, 35 pages, 2017.

[54] Y. Zhou, Q. Wang, D. Shi, Q. Liang, and Z. Zhang, "Exact solutions for the free in-plane vibrations of rectangular plates with arbitrary boundary conditions," *International Journal of Mechanical Sciences*, vol. 130, pp. 1–10, 2017.

[55] Q. Wang, B. Qin, D. Shi, and Q. Liang, "A semi-analytical method for vibration analysis of functionally graded carbon nanotube reinforced composite doubly-curved panels and shells of revolution," *Composite Structures*, vol. 174, pp. 87–109, 2017.

[56] Q. Wang, X. Cui, B. Qin, Q. Liang, and J. Tang, "A semi-analytical method for vibration analysis of functionally graded (FG) sandwich doubly-curved panels and shells of revolution," *International Journal of Mechanical Sciences*, vol. 134, pp. 479–499, 2017.

[57] Q. Wang, X. Cui, B. Qin, and Q. Liang, "Vibration analysis of the functionally graded carbon nanotube reinforced composite shallow shells with arbitrary boundary conditions," *Composite Structures*, vol. 182, pp. 364–379, 2017.

[58] F. Pang, H. Li, Y. Du, Y. Shan, and F. Ji, "Free Vibration Of Functionally Graded Carbon Nanotube Reinforced Composite Annular Sector Plate With General Boundary Supports," *Curved and Layered Structures*, vol. 5, no. 1, pp. 49–67, 2018.

[59] H. Li, F. Pang, X. Miao, Y. Du, and H. Tian, "A semi-analytical method for vibration analysis of stepped doubly-curved shells of revolution with arbitrary boundary conditions," *Thin-Walled Structures*, vol. 129, pp. 125–144, 2018.

[60] J. Guo, D. Shi, Q. Wang, J. Tang, and C. Shuai, "Dynamic analysis of laminated doubly-curved shells with general boundary conditions by means of a domain decomposition method,"

International Journal of Mechanical Sciences, vol. 138-139, pp. 159–186, 2018.

[61] G. Jin, T. Ye, and Z. Su, "Structural vibration: A uniform accurate solution for laminated beams, plates and shells with general boundary conditions," *Structural Vibration: A Uniform Accurate Solution for Laminated Beams, Plates and Shells with General Boundary Conditions*, pp. 1–312, 2015.

[62] T. Ye, G. Jin, X. Ye, and X. Wang, "A series solution for the vibrations of composite laminated deep curved beams with general boundaries," *Composite Structures*, vol. 127, pp. 450–465, 2015.

[63] S. Hosseini-Hashemi, H. Rokni Damavandi Taher, H. Akhavan, and M. Omidi, "Free vibration of functionally graded rectangular plates using first-order shear deformation plate theory," *Applied Mathematical Modelling: Simulation and Computation for Engineering and Environmental Systems*, vol. 34, no. 5, pp. 1276–1291, 2010.